

**Implementing Dynamic Foot Shape Models to Improve
Spacesuit Boot Fit**

by

Abhishektha Boppana

B.S., Case Western Reserve University, 2017 M.S., University of Colorado
Boulder, 2019

A thesis proposal submitted to the
student's graduate committee in partial fulfillment
of the requirements for the degree of
Doctor of Philosophy

Ann and H.J. Smead Department of Aerospace Engineering Sciences
2020

Committee Members:

Allison P. Anderson, Chair
Dr. Torin Clark
Dr. David Klaus
Dr. Rodger Kram
Dr. Dan Feeney

Boppana, Abhishektha (Ph.D. Aerospace Engineering Sciences)

Implementing Dynamic Foot Shape Models to Improve Spacesuit Boot Fit

Thesis directed by Dr. Allison P. Anderson

Abstract will be written in the future.

Contents

Chapter

1	Motivation	2
1.1	EMU Spacesuit Injury Incidence	3
1.1.1	Spacesuit Contact Injuries	3
1.1.2	Spacesuit Musculoskeletal Injuries	5
1.2	Hypothesized Spacesuit Injury Mechanisms	5
1.3	Spacesuit Injury Countermeasures	6
2	Background	7
2.1	Gas Pressurized Spacesuit Characteristics	7
2.1.1	An Inherently Stiff Structure	7
2.1.2	Mobility Design Features	8
2.2	Planetary Ambulation	9
2.3	Spacesuit Mobility	11
2.3.1	Modeling Spacesuit Effects on Mobility	11
2.3.2	MK III Ambulation Cost of Transport Factors	11
2.3.3	MK III Ambulation Effect on Walking Biomechanics	13
2.3.4	Subjective Feedback on MK III Ambulation	13
2.4	Spacesuit Fit	14
2.4.1	Spacesuit Sizing and Fit Process	15

2.4.2	Human Body Characterization for Fit Checks	15
2.4.3	Quantifying Fit	16
2.4.4	Effects of Fit on Performance	17
2.5	Summary	19
3	Investigative Rationale	20
4	Specific Aim 1 : Quantifying heel-lift during gait in the spacesuit	23
4.1	Introduction	23
4.2	Methods	23
4.2.1	IMU Data Filtering	24
4.2.2	Step Segmentation	26
4.2.3	Foot-flat Phase Detection	30
4.2.4	Zero Velocity / Zero Position Update	32
4.2.5	Outlier Step Removal	37
4.3	Results	37
4.4	Summary	38
5	Specific Aim 2: Predictively modeling dynamic changes in foot morphology during gait	43
5.1	Introduction	43
5.2	DynaMo: Dynamic Body Shape Capture with Intel RealSense Cameras	45
5.2.1	Background	45
5.2.2	Methods	45
5.3	Development of a Predictive Dynamic Foot Shape Model from Statistical Shape Modeling	49
5.3.1	Methods	49
5.3.2	Results	58
5.3.3	Foot Shape Changes	65

5.3.4	Study Limitations	67
5.4	Instep Height and Girth Analysis	68
5.5	Summary	68
6	Specific Aim 3: A design methodology integrating shape modeling into planetary spacesuit boot design	70
6.1	Introduction	70
6.2	Existing Knowledge on Foot Shape Mobility	70
6.2.1	Linear Anthropometry	71
6.2.2	Gait Joint Kinematics	72
6.3	Biomechanical Boot Design Framework	73
6.3.1	Mobility	74
6.3.2	Toe box	75
6.3.3	Upper	77
6.3.4	Sole	78
6.4	Prototyping Construction Plan	79
6.4.1	Design Process	79
6.5	Summary	80
7	Specific Aim 4: Evaluation of prototype planetary spacesuit boot design for fit and comfort	82
7.1	Introduction	82
7.2	Test Interface Construction	83
7.3	Glovebox Testing	83
7.4	Stretch Testing Goals	84
7.5	Summary	84
8	Execution Plan	85
8.1	Timeline	85

8.2 Publication Plan	87
8.3 Academic Requirements	89
Bibliography	92

Tables**Table**

5.1 Enrollment groups based on reported height. 5 subjects were enrolled in each group	50
8.1 Peer-reviewed publications	87
8.2 Conference Presentations and Posters	88

Figures

Figure

2.1	Knee (left) and foot (right) trauma identified in the MK III following 10 km walkback evaluation. From Norcross et al. 2009	14
2.2	Heel-lift occurring during heel-off, as subjectively reported in the MK III. The poor fit and indexing in the boot and lower torso allows the heel to lift inside the boot during heel-off	18
4.1	Placement of IMUs and Padding	25
4.2	Raw Vertical Acceleration of Tibia and SLL IMU	27
4.3	High-pass filtered velocity of Tibia and SLL IMU	28
4.4	IMU pitch angle over time	29
4.5	Step segmentation through peak angle detection	31
4.6	DWT transformed signal which was thresholded and then inverse transformed into the signal	33
4.7	Stance phase detected by finding zero-acceleration points in each step	34
4.8	Heel lift measurement quantities between SLL and tibia IMUs	36
4.9	Heel-off lag distributions between all subjects and configurations	39
4.10	DWT transformed SSL and tibia vertical acceleration. The shaded regions represent the detected stance phases, with the right-most shaded portion being heel-off. As seen here, the SSL experiences a vertical acceleration before the tibia, causing “negative lag”	40

4.11 DWT transformed SSL and tibia vertical acceleration. The shaded regions represent the detected stance phases, with the right-most shaded portion being heel-off. As seen here, the tibia experiences a vertical acceleration before the SSL, which may lead to heel-lift	41
5.1 Sample frames collected by DynaMo showing dynamic shape capture	46
5.2 Capture setup of 6 Intel RealSense D415 Depth Cameras (circled in red) placed around a treadmill. The checkerboard shown was used to calibrate the cameras using the DynaMo package.	51
5.3 Flowchart of processing steps for statistical shape model creation	53
5.4 Coordinate system defined from registered scans. Anatomical landmarks are shown as black dots. The ankle joint's local coordinate system is shown in blue, the MTP joint's local coordinate system is shown in yellow, and the model's origin coordinate system is shown in red. Directions for each coordinate system are shown in bold text	57
5.5 Processed and registered scans of one subject during heel-off, shown 10 frames (.11 seconds) apart	59
5.6 Distribution of errors across the various prediction models leave-subject-out cross-validation results. Model RMSE mean and standard deviation are shown above each distribution	61
5.7 Each graph represents the predictor's effects on the shape mode by visualizing the model's normalized coefficients. Larger absolute values indicate a larger effect from the predictor on the shape mode.	62
5.8 Each shape mode's principal axis represented as a heatmap overlaid on the mean foot and shown from 4 different point-of-views. The darker regions represent vertices which are most correlated with the shape mode's principal axis, and therefore see deformations in the shape mode.	63

5.9	Foot shape deformation at +2 and -2 standard deviations along each shape mode's principal axis, overlaid on the mean foot. The point-of-view is set to highlight the major variance along each shape mode's axis.	64
6.1	Foot-specific measures which directly affect mobility and comfort	71
6.2	(Right) Inequality in distribution of equivalent shoe size between male and female, (Left) relationship between foot length and arch length; visualizations developed from the ANSUR II Dataset	72
6.3	Overview and classification of measurements to footwear design variables with representative shoe	74
6.4	Mobility and flexibility of joints needed in the spacesuit boot	76
6.5	Conceptual design of a boot's upper configuration with pressure bladder	78
6.6	Desired sole flexibility (red) matched with plantar foot contour at MTP joint	79
8.1	Gantt chart showing PhD timeline	86

Chapter 1

Motivation

The Apollo missions represent the last time humans set foot on another planetary surface, the Moon. Future human spaceflight missions are retargeting planetary surface exploration by sending astronauts back to the Moon and onward to Mars. Planetary missions' goals include but are not limited to performing scientific experiments, collecting geological samples, and constructing infrastructure to support human life. While many of these duties may be completed by robotic missions, human exploration still plays a key role in the success of planetary missions [34].

An important component of planetary mission design is extravehicular activity (EVA), where astronauts conduct their duties outside their habitat. During EVA, astronauts are subject to many physiological and environment factors, including reduced gravity loading, dust, radiation, and thermal environment. In addition, the planetary atmosphere is not sufficient to prove life support. Spacesuits are designed to both provide life support and help protect the astronaut against these extremes during an EVA.

Humankind's current planetary EVA experience is limited to a total of 78 hours over 15 Apollo missions [100]. During the Apollo missions, astronauts performed almost 10 hours of EVA in a 24 hour period without the assistance of a rover during Apollo 14, and 22 hours of EVA in a 36-hour period with the assistance of a rover during Apollo 17 [100]. Ambulation is one of the top priorities for planetary mission designs. The longest traverse performed on the lunar surface occurred during Apollo 12, where astronauts Charles Conrad and Alan Bean walked 1.8 km [100]. Apollo 15-17 missions involving a rover assumed astronauts would be able to walk 5 km in case of rover failure

[100]. Future planetary mission design assumes astronauts can walk up to 10 kilometers to return to their habitat, and that astronauts can perform 8-hour EVAs, with a limit of 12 hours of EVA per 24 hours and 24 hours of EVA per 7 days [34]. In addition, NASA's current planetary exploration plans focus on extended stays and colonization, increasing the mission time on the surface, and therefore increasing the total amount of EVA performed by an astronaut during their stay. Future planetary EVA missions will therefore need a spacesuit able to adequately and comfortably protect astronauts on these long duration missions.

1.1 EMU Spacesuit Injury Incidence

Crewmember difficulties with the spacesuit have existed since the first EVA, where Alexi Leonov had difficulties moving the suit to re-enter the spacecraft. Apollo astronauts have commented on the fatiguing reduced mobility of their spacesuits [109]. Gas pressurized spacesuits are known to be inherently stiff and rigid [98, 1, 112, 56], difficult to move [92, 4], and have the potential to cause injuries both during operations and ground-based training [128, 120, 109, 110, 25].

The prevalence of injury has been well studied in the era of on-orbit microgravity EVAs performed with the Extra-Vehicular Mobility Unit (EMU). Strauss [120] found that 24.6% of training sessions at the Neutral Bouancy Laboratory (NBL) between 2004 to 2006 study had reported injury symptoms. Viegas [124] found a 67.5% reporting rate of injury symptoms from astronauts training in the NBL between 2002 to 2003. An in-flight injury incidence of 0.24 was reported by Scheuring [111] for EVAs occurring on Space Shuttle flights 90 to 113. These injuries can be broken down into contact and musculoskeletal injuries.

1.1.1 Spacesuit Contact Injuries

Spacesuit contact injuries, including bruises and abrasions, have been the most reported operational injury mechanism in the US space program [109]. Contact injuries occur through repeated contact between the wearer and the spacesuit. High contact pressure between the wearer and spacesuit can lead to bruises, while shear can lead to abrasions [78, 20]. Reviewing reported

injury incidences shows that contact injuries are the most common injuries reported in the EMU [120, 124, 111].

The hands were the most frequently reported location of EMU contact injury symptoms in all three injury analyses. Hand contact injuries include fingernail delamination, abrasions, contusions, and nerve impingement [120, 124, 111]. These injuries have widely been attributed to the poor fit and unprotected contacts between the hand and the spacesuit glove [120, 124]. Viegas reports a specific mechanism where the high exertion required to actuate the glove results in dorsal displacement of the metacarpophalangeal joints, pushing the tops of fingers against the surface of the glove and causing inflammation [124]. EVA hand injuries have been reported since the Apollo era, with symptoms including from swollen and abraded joints that were at risk for ending the EVA [111].

Shoulder injuries, the second most common EMU injury location, occur during ground-based training in the NBL when the wearer is inverted in the suit [120, 124]. While the wearer may be neutrally buoyant, they are still under the effects of gravity. Therefore, they “fall” into the suit, and are now making contact with the hard upper torso (HUT). The combination of unprotected contact and high loading from supporting their own body weight results in shoulder contact injuries [120, 124].

The feet are the next most reported areas of in-flight EMU contact injuries in the spacesuit [111]. Traditionally, not much motion occurs in the lower torso of the EMU spacesuit due to its design targeting microgravity operations. The feet are normally restrained in a fixed foot restraint, while the astronaut performs tasks utilizing their upper body. One astronaut reports a “searing, knife-like pain” on their foot during on-orbit EVA which was unable to be rectified[111]. This resulted in a blister and decreased sensation on the foot’s dorsal surface, and was later attributed to having excess pressure bladder material in the boot [111]. Strauss [120] also reports contact injuries on the toes and dorsal surface stemming from the boot sizing insert, which does not adequately project the astronaut from contact from the foot restraint or bladder folds.

EMU Contact injuries also occur at the elbow, knee, and trunk [120, 111]. Injuries at wearer’s

elbows and knees are reported to come from rubbing against the convolute joints [120]. Injuries at the trunk are reported to occur from contact between the wearer's back and the Liquid Cooling and Ventilation Garment (LCVG) in the spacesuit [120].

1.1.2 Spacesuit Musculoskeletal Injuries

Musculoskeletal injuries, including muscle tears, strains, and inflammation, are severe injuries stemming from high exertion and poor joint programming in the spacesuit. Fatigue from high exertion may also lead to injuries.

EMU Musculoskeletal injuries have been reported in the hands, due to the high exertion needed to actuate fingers on the pressurized glove [124]. Fatigue may occur after many hours of completing EVA tasks [120, 111]. Similarly, the elbow joints in the EMU have also reportedly caused strains [120].

The most severe EMU musculoskeletal injuries have occurred at the shoulder [120]. Some of these injuries have manifested into rotator cuff tears, requiring surgical intervention [121]. These injuries were attributed to the shoulder being forced by the HUT into internal rotation to perform certain tasks. As a result, EMU wearers overuse their rotator cuff, which are normally only used to stabilize the joint, leading to injuries [128].

1.2 Hypothesized Spacesuit Injury Mechanisms

The contact and musculoskeletal injuries reported in the EMU can be linked to specific deficiencies in suit design and suit compatibility. Poor suit fit can directly contribute to contact injuries. Spacesuits in the Apollo era were custom tailored to each astronaut. However, as the astronaut corps grew, the EMU presented a modular sizing system, where differently-sized suit components had to be selected for each astronaut. Gaps between the wearer and the spacesuit could lead to excessive contact when the wearer moves and shifts inside the spacesuit [11]. Suit components which are too small can also cause higher contact pressures, leading to potential contact injuries. Opperman [95] found that higher hand circumferences have a larger incidence of fingernail

delamination in the spacesuit glove, while Charvat [26] found smaller hand circumferences to be a risk factor in fingernail delamination. This disagreement highlights how important and poorly understood fit is inside the spacesuit. Fit can also affect mobility; the poorly sized scye openings in the EMU's HUT limited mobility, leading to musculoskeletal injury following repeated motion [128].

Poor indexing between the wearer's joint and the spacesuit's joint is a related injury mechanism. Poor indexing can lead to contact injuries when joint centers drift out of alignment, causing rubbing against the suit during motion. This was seen in the elbow and knee for the EMU [120]. Poor indexing is especially evident in the EMU's hard-upper torso (HUT), where the design restricts the natural movement of the shoulder joint, and required alternative movement techniques to achieve similar joint orientations [128, 120, 111]. Poor indexing can require increased exertion to move the joint [84].

Pressurized spacesuit joints require more energy to move [4]. While design features aim to reduce the effort needed to bend joints [54], these joints are difficult to engineer in areas such as the hand. Therefore, the fatigue and strain injuries reported in the hand could be due to inherent design deficiencies of EMU spacesuit gloves [120, 124]. Increased humidity can also lead to fingernail de-lamination [25].

1.3 Spacesuit Injury Countermeasures

Attempts to mitigate spacesuit injury have focused on addressing the outlined injury mechanisms. No perfect countermeasure has been presented for poor fit, it still remains impossible to perfectly fit every person to the EMU spacesuit due to the wide ranges of anthropometry and limited sizing components [11]. Back padding on the EMU was found to potentially assist wearers in controlling the upper torso of the suit, reduce over-rotation of the torso to keep upper extremity joints aligned, and improve indexing at the gloves [25]. For wearers with a smaller anthropometry however, indexing at the hip bearings was unable to be fixed by padding, due to the limitations in torso length.

Chapter 2

Background

Many of the injuries identified in both operational and training environments have been concentrated around the shoulder/HUT interface, since the microgravity EVA environment is dominated by upper-body tasks. The transition to planetary missions will require much more walking, and therefore use of the lower torso, than current microgravity missions. Therefore, it can be expected that there will be a higher incidence of lower-torso injury in future planetary missions. While these specific injury mechanisms may not occur exactly as in the upper-torso, it is important to study and ensure proper human-spacesuit interaction for future high-use lower-torso spacesuit components. A risk analysis of injury and compromised performance during EVAs showed poor EVA suit design and poor EVA suit fit as two of the main suit design variables leading to risk [25]. This chapter introduces the existing knowledge on suit design, presents the current state of suit mobility as it relates to ambulation, and introduces the challenges with fitting spacesuits.

2.1 Gas Pressurized Spacesuit Characteristics

2.1.1 An Inherently Stiff Structure

Gas pressurized spacesuits have been used for all EVAs throughout the history of human spaceflight. However, gas pressurized suits become stiff and rigid when pressurized, requiring great effort to bend. The first EVA spacesuit, the Gemini suit, did not include any design features to reduce bending effort [?]. If a gas pressurized suit component is represented as a pressurized cylinder, bending the cylinder along its axis causes a reduction in volume at the bend [54]. As

a result, pressure at the bend will increase, causing resistance to the bending force. The force required to change the volume at the bend is presented as:

$$F = \frac{W}{d} = \frac{\frac{p\pi D^3 \phi}{8}}{\frac{L\phi}{2}} = \frac{p\pi D^3}{4L}$$

[89, 54], where F is the force required, W is the work required, d is the distance the joint is flexed, p is the pressure, D is the cylinder's diameter, ϕ is the joint deformation angle, and L is the length of the cylinder. It can be seen that the force required to bend a pressurized joint is not dependent on the bending angle, but rather the length and diameter of the pressurized section. Without dedicated mobility features to maintain a constant volume at joints, the forces required to bend representative spacesuit components can be as high as 200 lbs for the waist joint [89].

2.1.2 Mobility Design Features

Mobility features specifically designed to maintain constant volume through joint bending motions are needed to reduce bending resistance and allow for joint flexibility [54]. These mobility features typically feature some form of bellows or convolutes to maintain constant volume and axial restraints to prevent elongation under pressurization [54].

The Litton company built and tested spacesuits for EVA use in the 1950s, predating both the US and Russian space programs. These suits iterated on the use of convolutes by inventing the rolling convolute, annular convolute, and cardonic hard joint [54]. While these suits never saw operations on spaceflight, they did prove benefits in mobility over the International Latex Corporation (ILC) designed A7L suits, which were eventually used by US astronauts on the moon. The Litton suits were able to match the center of restraint and center of pressure when convolute joints were bent, reducing the bending torque and spring return force of the joint [54]. Therefore, the suit's operator is able to easily bend the joint and not exert much force to keep the joint bent. The A7L suit's convolute joints did not match the center of restraint and center of pressure, requiring operators to exert additional force to both bend the joint and keep it bent [54]. Such drawbacks of the A7L suit required astronauts to come up with clever workarounds. On an Apollo

16 EVA, astronaut John Young found that “by hopping into the air and landing on his feet, the weight of his suit overcame the suit’s internal pressure, so he could get to his knees and pick up rocks without using geological tools” [100].

Advancements since the Apollo era have brought us improvements in pressurized joint design to increase mobility, including the toroidal mobility joint, dual-axis joint, hard component joints, hybrid hard-component/fabric joints, and improvements to flat-patterened joints [54]. The Mark III Advanced Space Suit Technology Demonstrator EVA Suit (MK III) is a spacesuit designed by NASA as a planetary spacesuit design testbed [68]. These advancements have allowed for increased lower-torso mobility as shown in the MK III spacesuit technology demonstrator; operators are easily able to recover from a fall and kneel in the MK III while these tasks were done with much difficulty in the A7L and EMU spacesuits [67].

Lessons from EMU and MK III design have been applied to new planetary Z2 spacesuit. Subjects found mobility improvements for the upper torso to have improved with the Z2 spacesuit [83]. The Z2 spacesuit features a larger scye opening and more mobile shoulder bearings to help with mobility [51]. However, subjects still reported fit issues, and similar muscle fatigue and exertion ratings between the EMU and Z2 [83]. Limitations with the fit and mobility of the spacesuit still pose a risk for injury.

2.2 Planetary Ambulation

Astronauts during the Apollo missions famously did not ambulate in a typical walking fashion; they famously loped across the surface. In fact, loping is the energetically preferred gait on the Lunar surface, while walking, skipping, and running are energetically preferable on Mars [2]. As speeds increase in lunar gravity, a transition occurs from walking to skipping rather than from walking to running as on Earth [85]. However, the energetically preferred speed is not always achievable or possible, especially when performing EVA tasks, and slow walking speeds may be necessary.

Walking is modeled as an inverted pendulum which conserves some energy between each

step; but energy is not conserved at faster walking speeds and needs muscular power input [23, 22]. Griffin et al [52] found as gravity is reduced, the amount of mechanical energy conserved between each step is reduced, and the maximum energy recovery occurs at slower speeds. Ivanenko et al [57] found that muscle activation and ground contact forces decreased with lower gravity levels, but kinematic coordination of the lower limbs were not affected by gravity levels.

Studying the walk-run or walk-skip transition gives further insight into ambulation on a planetary surface. The Froude number is the ratio between the centripetal and gravitational forces in the inverted pendulum model :

$$Fr = \frac{v^2}{gL}$$

Where Fr is the Froude number, v is the velocity of ambulation, g is the gravitational force, and L is the leg-length [?]. At some critical value, walking is impossible as the gravitational force cannot match the required centripetal force, which is where the walk-run transition occurs (Fr^*). Humans typically switch to running at $Fr = 0.5$. Kram et al [70] offloaded subjects by their waist as they walked and ran on a treadmill, and found that Fr^* increases at lower gravity levels. The increase in Fr^* was hypothesized to be from the arms and legs not being offloaded and still under the influence of gravity [70]. Donelan and Kram [33] also found that elastic forces were unable to predict the dynamics of reduced-gravity running. This suggests that other factors may be at play with walking in reduced gravity.

Newman and Alexander [90] suggested that energy may be expended at low speeds and lower gravity levels for stability and postural control for ambulation. Chappell [24] found that when the offload system was set to lock waist rotation for stability, subject's gait was constrained and showed changes in braking and propulsion force for Lunar gravity. Therefore, stability is an important factor in walking at lower gravity levels.

2.3 Spacesuit Mobility

2.3.1 Modeling Spacesuit Effects on Mobility

Carr and McGee [21] developed the Apollo number Ap to explain the effects of spacesuit on gait:

$$Ap = \frac{Fr}{M}$$

where M is the mass ratio of the spacesuit. M incorporates the self-supported weight of the spacesuit. The self-supported weight of the spacesuit is from the spacesuit's pressurization. Carr and McGee validated the Apollo number against gait events during Apollo missions, but found that the Apollo number did not fully explain the walk-skip transitions. Therefore, spacesuit's mobility restrictions and joint mechanical work may also be affecting the walk-run transition.

2.3.2 MK III Ambulation Cost of Transport Factors

Due to the Z2's relative novelty, most spacesuit ambulation studies have been conducted with the MK III spacesuit. In the EVA Walkback Test (EWT), six male subjects were tested with the MK III spacesuit on a treadmill to explore the effects of the MK III spacesuit's weight on planetary walking in Lunar (1/6g) and Martian (3/8g) gravity levels.. Subjects were tested in three conditions: unsuited and offloaded to selected gravity level; unsuited and offloaded to selected gravity level with the suit weight matched; and suited while offloaded to selected gravity level[92]. This allowed for analysis of suit weight separately from other suit design factors on the metabolic cost of suited walking. Subjects were tested at three speeds above and three speeds below their walk-run transition speed. All subjects also did a 1G baseline unsuited trial and a 10 km suited lunar ambulation. A follow-on integrated suit test (IST) examined the effects of varied suit mass, gravity, and on metabolic cost and kinematics on Lunar suited gait [91] with similar conditions while varying suit pressure and mass.

Metabolic cost of transport, a measure of how much energy the body is exerting during ambulation calculated through direct calorimetry [62], was collected for a variety of conditions.

Metabolic cost is a direct measure of how hard the body is working to move in the spacesuit. Previous studies have shown that the metabolic cost of transport decreases with gravity [48].

Findings from the EWT and IST were consistent with these previous findings [92, 91]. Unsuit weight-matched metabolic costs were lower than 1G unsuit across all speeds for 1/8G ambulation and similar to 1G unsuit for 3/8G ambulation [92]. This suggests that without suit effects, walking on Mars may be metabolically similar to walking on Earth. However, the MK III increased the metabolic cost of transport for both gravity environments compared to the unsuit weight-matched condition [92]. At 1/6G, the MK III had a higher metabolic cost than Earth ambulation at lower speeds, but was less metabolically costly at higher speeds [92, 91]. The MK III was very metabolically costly in 3/8G, metabolic cost quickly approach maximal values for low speeds and subjects were unable to run in the suit at higher speeds [92]. The metabolic cost of weight (5%-13%) for both Lunar and Martian gravity levels was significantly dwarfed by the cost of suit design factors (87%-95%) [92]. From these results, its apparent that the MK III cannot service ambulation Mars due to its design factors, but may be sufficient for the Moon.

The IST found increased suit pressure to minimally increase metabolic cost across all speeds, hypothesized to be due to the constant volume joints of the MK III [91]. However, there were some subjective differences in mobility noted across the different pressures, although there was no correlation to subject anthropometry [91]. The effect of suit weight, which encompasses gravity level and suit mass, steadily increased with speed [91]. The percentage of metabolic cost that was not explained by suit weight or pressure decreased as speed increased, but then increased at the fastest speed [91]. These factors can include suit kinematics, stability, and harnessing effects from the gravity offloading, which may be causing more difficulty for ambulation at lower speeds. The majority of ambulation during an EVA is most likely done at lower speeds, thereby requiring further understanding of how suit design is affecting mobility at low speeds.

2.3.3 MK III Ambulation Effect on Walking Biomechanics

The IST captured little differences in kinematics as a function of pressure, which may be due to the constant volume joints [91]. However, it was noted that at 4.3 psi, the knee joint was limited by the design of the pressurized suit, and that the ankle increased its range-of-motion (ROM) to compensate the limited knee ROM [91]. This shows the importance of the kinematic chain in suited mobility; when a certain motion is inhibited, other joints along the kinematic chain will have to compensate. Similar compensation has led rotator cuff injury in the EMU's HUT [128].

Cullinane et al [30] found suited MK III ambulation at 1G to reduce heel and toe clearance above ground compared to unsuited walking. In addition, the MK III was found to decrease speed, stride length, and step length compared to unsuited walking [30]. Cadence and stance time increased with gravity level in the IST, consistent with how metabolic cost increases with gravity level [91]. These findings suggest that the MK III inhibits operator mobility and agility when walking.

2.3.4 Subjective Feedback on MK III Ambulation

Subjective feedback allows operators of the MK III to provide their perception of walking in the suit. Rating of Perceived Exertion (RPE) and Gravity Compensation and Performance Scale (GCPS) were consistent with metabolic cost findings in both the IST and EWT; both increased with gravity and speed [92, 91]. Subjects performing the 10 km walkback in the EWT reported “fair” to “moderate” operator compensation required to walk in the MK III on the Cooper-Harper Scale[92]. While mean rating of discomfort was “very low” to “low” on the Corlett-Bishop Scale, discomfort and trauma were noted on the knees and feet of some subjects [92] fig. 2.1. In addition, muscular fatigue and tightness was also reported in the quadriceps, thighs, glutes, and lower back [92].

Subjective feedback for walking in the MK III at 1/6-g suggests that it is mostly acceptable. However, the reported trauma and musculoskeletal discomfort are areas of concern. The EWT and IST, along with findings from Cullinane, show that the MK III's design inhibits natural human

motion and requires more effort to walk in. However, it is not enough to make a suit that is more mobile; it also needs to work closely with its operator.



Figure 2.1: Knee (left) and foot (right) trauma identified in the MK III following 10 km walkback evaluation. From Norcross et al. 2009

2.4 Spacesuit Fit

Human-spacesuit interaction is driven by how well the spacesuit fits around its operator. Contact and musculoskeletal injuries stem from inadequate static and dynamic fit between the spacesuit to the human. Static fit refers to the alignment between the operator and the spacesuit, while dynamic fit refers to the coordination of the operator to the spacesuit during motions [119]. Poor static fit leads to empty space around the operator, which allows the operator to move inside and repeatedly contact the spacesuit. However, improving static fit is not as easy as filling this empty space; this would hamper operator mobility and lead to poor dynamic fit and difficulty for the operator to move the suit. Poor spacesuit-operator fit is a factor of both difficulty in sizing the suit to the crewmember, ensuring that suit movements match desired human movements, and understanding human body shape.

2.4.1 Spacesuit Sizing and Fit Process

The Apollo EVA spacesuits were custom tailored for each individual, a feat achievable with the small number of astronauts needing EVA suits [54]. However, with a larger and more diverse astronaut corp, custom suits became infeasible. Currently, only the EMU glove is custom made if one which fits the astronaut does not exist [25].

NASA STD-3000 calls for spaceflight hardware to accommodate an anthropometric range from the 5th-percentile female to the 95th-percentile male [87]. The EMU suit was designed to target this range with modular and adjustable components. Table XX shows the number of modular component available for the EMU [66]. However, the EMU design only ended up fitting a 40th-percentile female to a 95th-percentile male [64]. Current suit fit processes do not use any objective measures to define proper fit; a baseline fit is prescribed from anthropometric measures and then iterated through subjective feedback [38].

Sizing rings are used in the EMU design to change the length of components like arms and legs [54]. Sizing inserts such as pads can also help position the operator within the spacesuit [25]. The length of restraint straps at convolute joints can be adjusted to change the length of soft components, but this affects joint mobility as the length-diameter ratio is modified [54].

2.4.2 Human Body Characterization for Fit Checks

NASA's Anthropometry and Biomechanics Facility (ABF) has focused on characterizing the human body as it relates to spacesuit fit. Linear measurements are traditionally used in sizing algorithms to determine a baseline suit fit. These linear measurements are then compared to linear measurements in the suit's design to determine appropriate sizing components. However, linear measurements do not always accurately represent a person's body shape [80]. Three-dimensional scanning can help accurately characterize body-shape to allow for virtual fit testing against 3D models of the suit. Boundary manikins can be generated which represent the extremities of accommodated anthropometry, and overlaid on 3D suit models to determine fit [80]. Virtual fit check

metrics may include penetration depth, contact areas, and overlap volume [64]. Monte-Carlo simulations of vast databases can also be virtually tested to find fit problems that may occur outside the boundary manikins [64].

It is well known that parts of the body change shape during movement. Capturing 3D-scans in multiple poses also allows for the development of a parametric models that can estimate how body shape changes with a specific movement; for example this can be used to check shoulder clearance around the HUT [65]. This can greatly improve dynamic fit as it ensures the HUT accommodates the shoulder throughout its entire motion. However, this methodology is limited to poses where the subject can pause between motions due to technological limitations for capturing dynamic body shape changes.

Body shape changes can also occur from exposure to an altered-gravity environment. The ABF found on average posture to increase by a maximum of 3%, hip circumference to decrease by a mean of 7%, and thigh circumference to decrease by a mean of 10% during microgravity spaceflight [64]. EMU sizing incorporates a 2.54cm increase in torso length to accommodate this change [122].

Information from virtual fit testing can be incorporated into spacesuit design by informing where the internal geometry may need to be expanded or contracted to better fit the target population [64]. This process was used to validate the design of the Z2 suit. However, it is virtually impossible to incorporate personal preferences of fit into this process; currently a threshold is implemented to determine acceptable levels of ease or compression [64]. In addition, modifying design to accommodate findings from fit can only be done to a certain extent; there are limitations on modifying the structure of an existing design while still meeting the same engineering requirements. There are also no clear metrics for translating virtual fit testing into spacesuit component design. Therefore, fit will still need to be validated with the target population before being acceptable.

2.4.3 Quantifying Fit

Quantifying fit relies on measuring human motion inside the spacesuit, which is difficult as traditional-motion capture techniques do not work. Pressure sensors can help quantify contact

between the operator and spacesuit [5]. Inertial-measurement unit systems aim to provide some insight into in-suit motion [13, (author?) [115]]. Fabric strain sensors have also been developed to predict body-shape inside the spacesuit [64].

Fineman et al. [39] introduced two objective fit metrics: difference in knee angle ROM between the suit and operator, and the relative coordination metric [40]. The relative coordination metric allows for the identification of whether the suit or the operator is driving the other component. However, both of these metrics require measuring human movement inside the spacesuit.

2.4.4 Effects of Fit on Performance

The effect of fit on performance needs to be quantified to properly implement and understand objective fit metrics. The ABF found that a back pad could improve controllability of the EMU's upper body [25].

Fineman et al. [39] studied the effects of fit on MK III ambulation using objective fit metrics. Three subjects walked in a spacesuit with different levels of padding, meant to mimic three different levels of fit. Two subjects had reduced knee ROM compared to unsuited ambulation. One subject had no significant differences in metrics between padding levels but reported better responsiveness with higher levels of padding. Another subject had the lowest knee ROM with no padding, aligning with their feedback that higher levels of padding are harder to control. Suit fit engineers have commonly reported a dynamic fit problem where the heel lifts out of the boot during heel-off, which was also reported by one subject in the study [39]. fig. 2.2 shows how heel-lift can occur through poor fit and indexing. Data collected from Fineman's study shows that during heel-off, the suit appears to be driven by the wearer at the calf, which could be an indication of heel-lift. Fineman et al [39] suggests that boot fit may be very important to walking in the MK III, and that the objective fit metrics presented are sensitive to small changes in fit.



Normally , the heel is secured in the boot

However, during gait the heel can lift before the boot, resulting in a gap (shaded)

Figure 2.2: Heel-lift occurring during heel-off, as subjectively reported in the MK III. The poor fit and indexing in the boot and lower torso allows the heel to lift inside the boot during heel-off

2.5 Summary

Walking on another surface and gravitational environment presents many challenges of its own, including changes in preferred gait patterns. Wearing a stiff, pressurized spacesuit further increases the effort required to walk. While constant volume joints may reduce pressurization effects, unquantified factors such as joint torques and poor operator-spacesuit interaction may also be leading to injury.

Fitting a diverse range of persons to the spacesuit also faces challenges including limited suit sizing components, limited suit design flexibility, an incomplete understanding of body shape changes, and lack of objective fit metrics to validate fit. Poor fit has the ability to reduce performance in the spacesuit by affecting how the operator moves the suit. Ambulation specific fit issues, such as heel-lift, have been subjectively identified in the MK III but not fully quantified. While there has not been a large scale study on injuries in the MK III, these fit issues may lead to injury in similar mechanisms as noted in the EMU.

Chapter 3

Investigative Rationale

Matched fit and mobility must be ensured by suit design to ensure safe, comfortable planetary ambulation. Ideally, the spacesuit should require minimal additional exertion or change in movement strategies to ambulate compared to ambulating on Earth. To achieve this, spacesuit components should be the shape of the operator's body throughout their entire motions. Currently, spacesuit mobility is designed around the achievable mobility range first, and then fit to the operator's body type second. Dynamic body-shape models provide insight into how the body changes shape through moves and changes shape, have the ability to improve compatibility between the spacesuit and operator, and provide better static and dynamic fit, but have only been used in a limited fashion with the Z2 shoulder design. No clear process exists for integrating dynamic body-shape models into the spacesuit design process.

This proposed thesis will investigate the applicability of body shape models to improve fit and comfort for planetary EVA suit design. To limit the scope of the work, the proposed work will focus on fit and mobility of the spacesuit boot. The MK III spacesuit currently uses a pressurized modified hiking boot with a convoluted ankle joint and boot sizing inserts. The boot is an important component for MK III ambulation and MK III boot fit has been identified as a key issue in suit fit [39]. While the thesis will focus on the foot-boot interface design, the novel contribution lies in the development of a experimental and design framework to translate body-shape changes into spacesuit design variables. The proposed hypothesis of this work is therefore:

Integrating dynamic body shape changes into the spacesuit boot design process

will mitigate factors that lead to injury and improve compatibility between the operator and the spacesuit.

The proposed thesis will encompass the following specific aims:

- Specific Aim 1: Quantify heel-lift in spacesuit gait
 - * Motivation: Heel-lift was subjectively reported as a potential symptom of poor fit during gait in the MK III, but was never quantified. Quantifying the level of heel-lift may lead to heel-lift can better inform boot design to mitigate this issue.
 - * Summary of Work: Walking data was collected on the MK III by Fineman et al. [2018]. This data was reanalyzed in the context of boot fit by analyzing vertical accelerations of the spacesuit's lower leg and operator's tibia. Heel-off times were detected using vertical accelerations. An analysis was conducted on quantifying displacement from vertical accelerations, but was found to have large margins of error. Therefore, this work proposes differences in heel-off times as an indicator of heel-lift.
- Specific Aim 2: Predictively model dynamic changes in foot morphology during gait with statistical shape modeling
 - * Motivation: The foot changes shape during the loading process of stance phase. Modeling these changes as they relate to subject anthropometry and kinematics will allow for prediction of dynamic foot shape during stance phase.
 - * Summary of Work: A novel dynamic foot scanning system was developed to capture 4D foot scans from subjects walking on a treadmill. Dynamic foot scans were captured from thirty subjects as they walked on the treadmill. A predictive statistical shape model was developed to predict dynamic foot shape with an accuracy of 5.2 mm. From the model, the midfoot was found to decrease in girth as the foot is lifted through heel-off. Dynamic changes in the midfoot will be further studied across the population as it relates to instep height and instep girth.

- Specific Aim 3: Develop a design methodology to integrate shape modeling into planetary spacesuit boot design
 - * Motivation: Existing knowledge on foot mobility can provide mobility requirements for a planetary spacesuit boot. Insight from the dynamic foot shape model can be integrated with these mobility requirements to develop a boot design that accommodates the mobility and dynamic shape of the boot.
 - * Summary of Work: Mobility of the foot was characterized from the existing literature. A biomechanical design framework was developed to integrate these mobility requirements with the dynamic foot shape model developed in Specific Aim 2. This framework will be used to create a pressurized planetary spacesuit boot prototype. The prototype boot will be constructed and sized for one specific subject.
- Specific Aim 4: Evaluate a prototype planetary spacesuit boot design for fit and comfort
 - * Motivation: The planetary spacesuit boot design developed in Specific Aim 3 will be tested for improved fit and comfort as compared to a current MK III spacesuit boot design and a non-pressurized standard hiking boot. This will directly test the hypothesis of this thesis.
 - * Summary of Work: The test subject will perform ROM tests in a glovebox with a vacuum, which will pressurize the boot. The subject will also perform heel lifts against a false floor simulate the heel-off phase of gait. Kinematics of the ankle and MTP joint will be captured. A contact sensor in the heel of the footwear will check for the heel-lift. Subjective surveys will assess the subject's fit and comfort levels. If the prototype boot design can achieve pressurization around the foot outside the glovebox, gait kinetics and kinematics will be captured with all three designs. The prototype boot may also be tested in conjunction with a full spacesuit, pending spacesuit testing availability.

Chapter 4

Specific Aim 1 : Quantifying heel-lift during gait in the spacesuit

4.1 Introduction

Heel-lift is a subjectively reported fit issue with the MK III spacesuit boot; the operator's heel inside the boot lifts inside the boot before the heel of the boot lifts at heel-off [39]. Quantifying heel-lift's kinematics will provide insight into its mechanism.

The data collected by Fineman et al [39] used inertial measurement units (IMUs) placed on corresponding locations of the operator's and MK III's lower torso. IMUs measure the acceleration and orientation of the segment they're attached to, but can be subject to error in the spacesuit environment [13, 115, 116]. Heel-lift can be characterized as the delay of heel-off between the human and spacesuit; essentially, the human experiences heel-off prior to the spacesuit doing so. IMUs have been widely used in the biomechanics field to detect heel-off points during gait [102, 41].

Therefore, this work's objectives include:

- detect heel-off times of both the spacesuit and the operator using the IMUs to detect the presence of heel-lift.
- measure the amount of heel-lift experienced by the human
- identify the relationship between lower torso fit and heel-lift

4.2 Methods

Experimental data collected by Fineman et al [39] was reanalyzed for this study. Three subjects walked along a 10m walkway for 24 trials in each of four conditions: unsuited, MK III with no padding, MK III with low padding, and MK III with high padding. All three subjects wore the same size MK III lower-torso, but Subject 3 wore a BOA-laced boot while other subjects wore

a standard strap-laced boot. Padding and IMU locations are shown in fig. 4.1.

Operator IMU Placement	Spacesuit IMU Placement
sacrum	bottom of HUT
right thigh	right upper leg
left thigh	left upper leg
right shank	right lower leg
left shank	left lower leg

The right and left shank/lower leg IMUs' vertical acceleration and Euler pitch angles were analyzed. Figure XX shows the overall workflow of this analysis, with details outlined in the sections below.

4.2.1 IMU Data Filtering

4.2.1.1 Acceleration Data

Vertical acceleration data is de-trended to remove bias by removing the best straight-fit line from the data vector. A low pass-filter reduces high-frequency noise in the signal. Antonsson and Mann (1985)[7] found that 98% of the signal power in gait's vertical amplitude was contained below 10 Hz. Therefore, the data was filtered with a 5th-order low-pass Butterworth filter with a cutoff frequency of 10 Hz. A moving-average filter is used to smooth the dataset, remove any noise left from low-pass filtering. The moving average filter is widely used to detect gait-events from IMU data[53]. A moving average filter produces a similar response to a low-pass filter. A window of 30 samples (.23s) is used; this value was found through trial-and-error. A 30-sample window is approximately equal to a ~4Hz low-pass filter. This window is within the range of windows used for walking-speed estimation [19].

The vertical velocity of the tibia and SLL is derived by integrating the de-trended, down-sampled, and low-pass filtered vertical acceleration IMU data. The unfiltered vertical velocity if

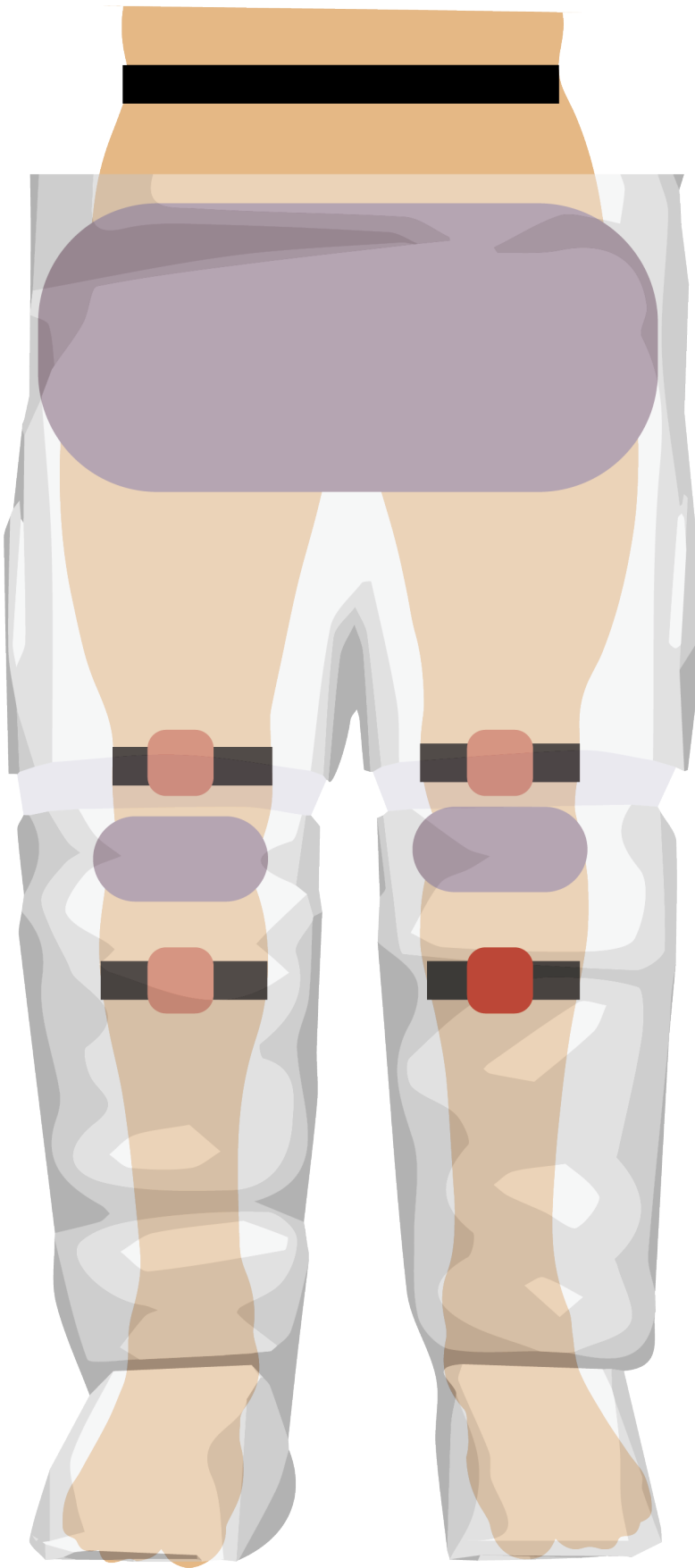
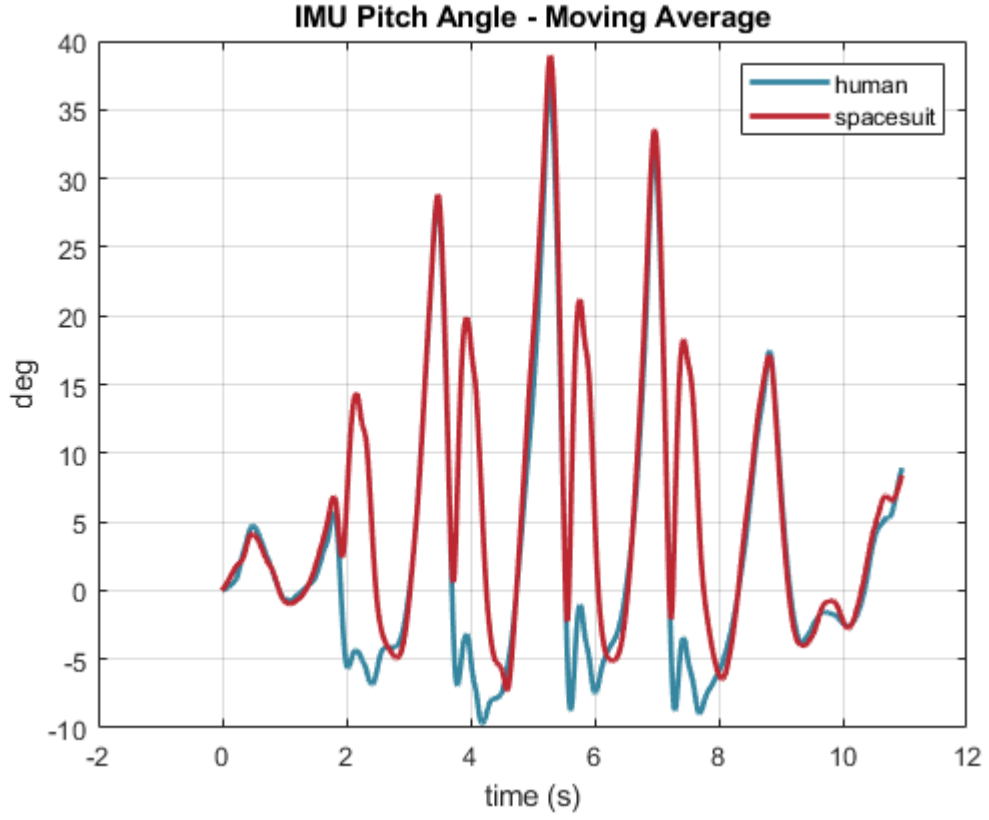


Figure 4.1: Placement of IMUs and Padding

shown in fig. 4.2 However, simple integration introduces drift. Therefore, a high-pass filter is implemented prior to the integration of the acceleration data to reduce drift, which occurs at a fairly low frequency ($<<1\text{Hz}$) [114]. The data was filtered with a 5th-order high-pass Butterworth filter with a cutoff frequency of 0.7Hz [105]. The filtered data is shown in fig. 4.3.

4.2.1.2 Angular Data

The unprocessed pitch angle is shown in fig. 4.4. The pitch angle is normalized to it's first value in the time series for each trial. A moving average filter with a window of 10 samples, set through trial and error, was used to smooth the pitch angle, and is shown in fig. ??.



{fig. ??}

4.2.2 Step Segmentation

Each step taken by the subject was identified using detected peaks in pitch angle of the IMUs. These peaks are thought to correspond to the max posterior flexion/extension of the tibia/SLL during the swing phase. The parameter **MinPeakDistance** is set to 1.5s to ensure high-frequency

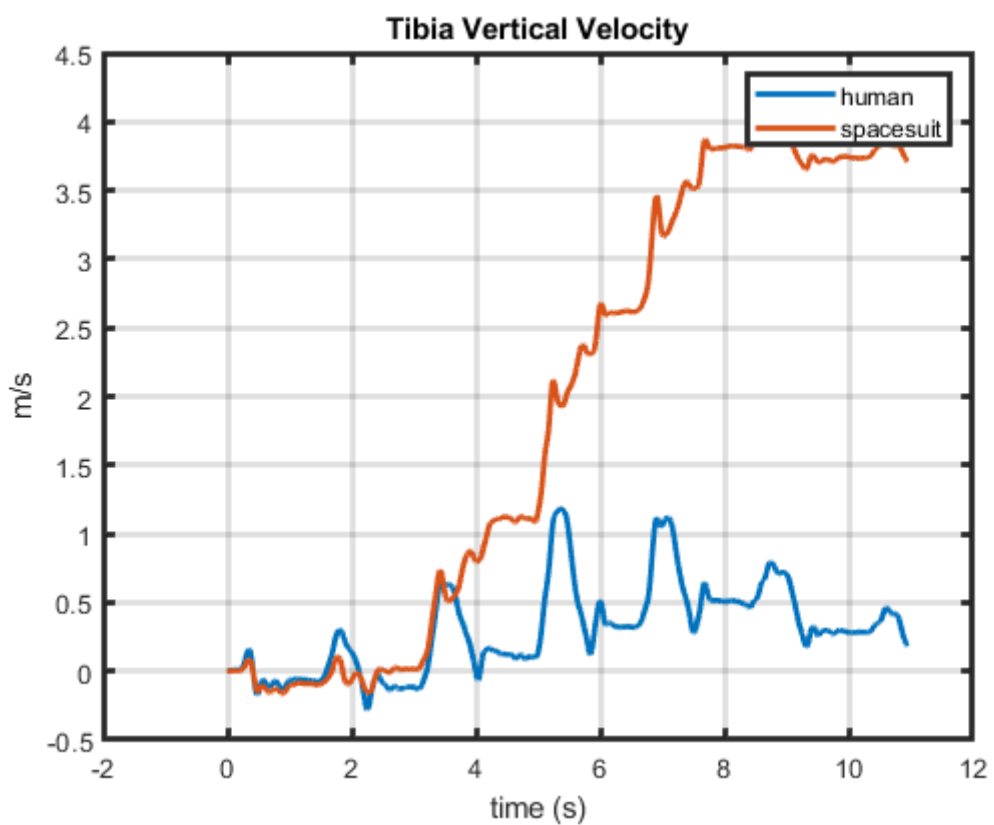


Figure 4.2: Raw Vertical Acceleration of Tibia and SLL IMU

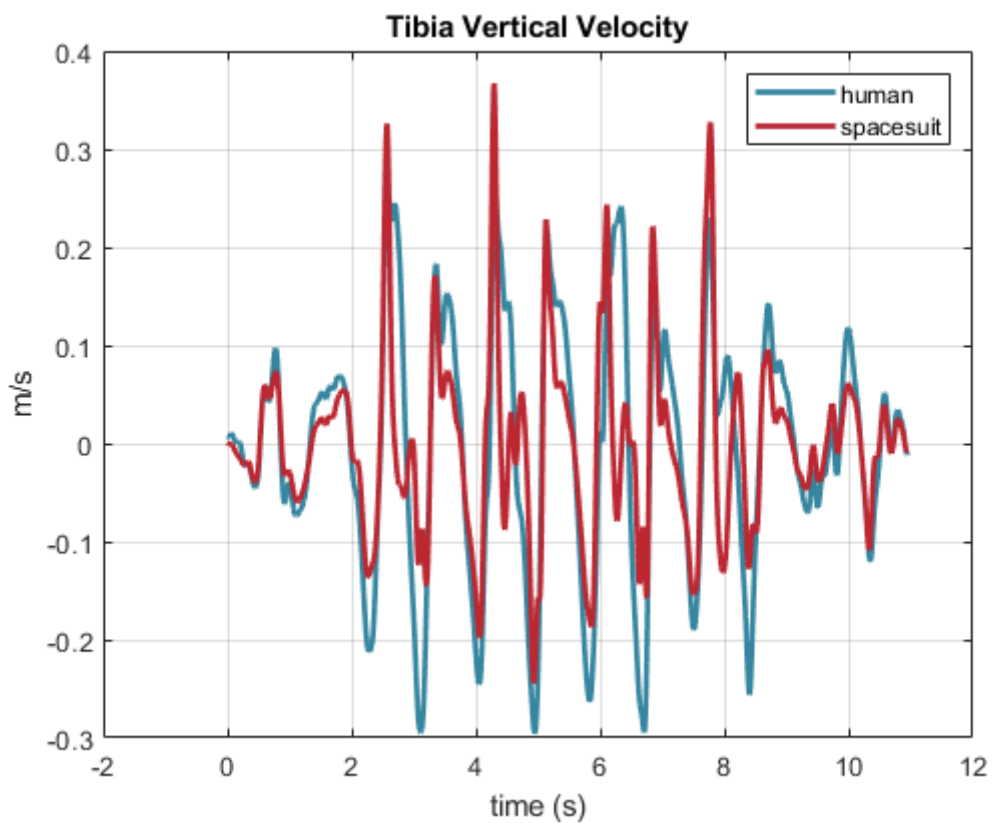


Figure 4.3: High-pass filtered velocity of Tibia and SLL IMU

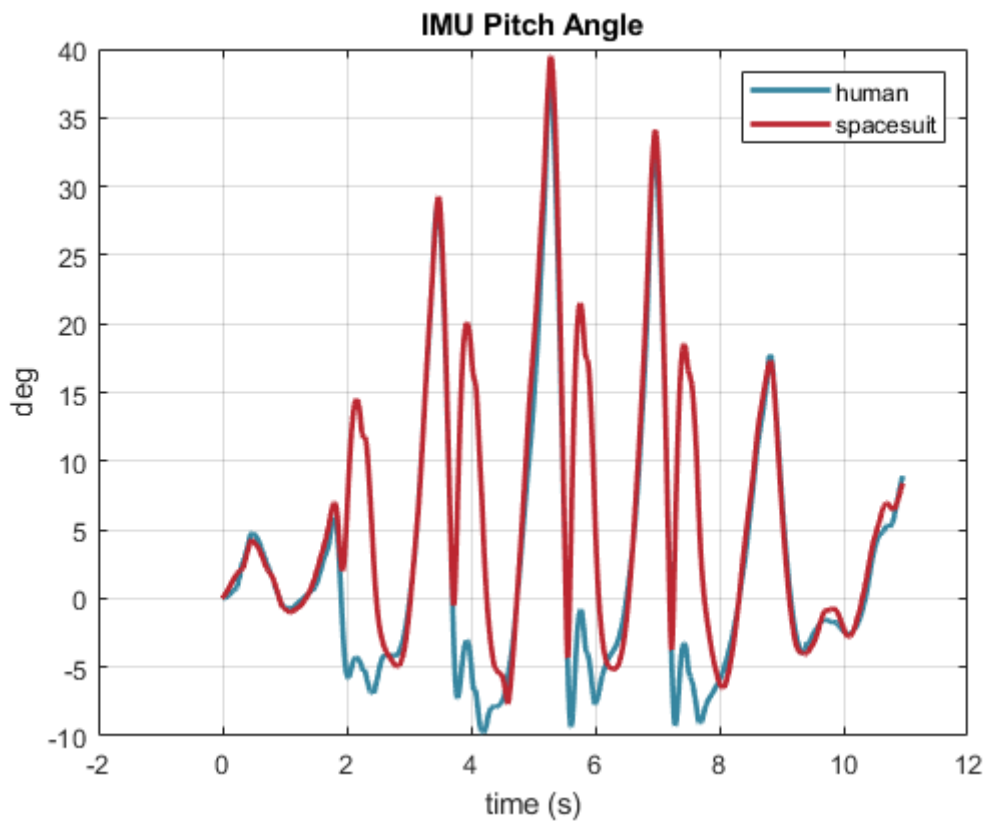


Figure 4.4: IMU pitch angle over time

peaks are not detected; this parameter was set based on the observed length of each step typically taking longer than 1.5s.

Since the first and last peaks of the trail may not be complete steps, they were not included in the analysis. The parameter **MinPeakProminence** is set to 0.40 radians (23 degrees) to ensure that the first and last peaks of the steps are not detected, as they were observed to be lower than this value across all trials. Peaks which corresponded to complete steps were observed to be closer to 0.60 radians (35 degrees). Each step is defined as the time between each step's max extension to the following step's max extension. An example of the step detection for a single trial is shown in fig. 4.5.

Once the locations of the peaks are detected, they are reshaped into an array which represents the start and end indices of each step. Since the peak detection is not a perfect algorithm, the number of steps detected in one trial for the SLL and tibia might not be the same. Therefore, whichever IMU had the least amount of steps detected has its step times applied to the other IMU. However, this is a very rare occurrence (<10 trials), occurring only when a step may not meet the **MinPeakProminence** threshold for either the tibia/SLL IMU, while meeting the threshold for the other.

4.2.3 Foot-flat Phase Detection

The foot-flat phase is the time duration between toe-strike and heel-off, where the foot is flat on the ground. This phase is characterized by very low anterior-posterior acceleration; since the foot is flat on the ground, there is very little vertical movement of the shank [102]. To more accurately identify this phase, a 3-level discrete wavelet transform (DWT) is applied to the de-trended, low-pass filtered, smoothed human and spacesuit anterior-posterior acceleration signals. The DWT works as a cascading filter bank at each level, simultaneously low-pass and high-pass filtering. A `sym2` Symlet is used as the mother wavelet for the transform, due to its high performance in detecting initial-contact and final-contact points during stance phase [58]. After transforming to wavelet space, a threshold is applied where values below 2% of the maximum wavelet coefficient

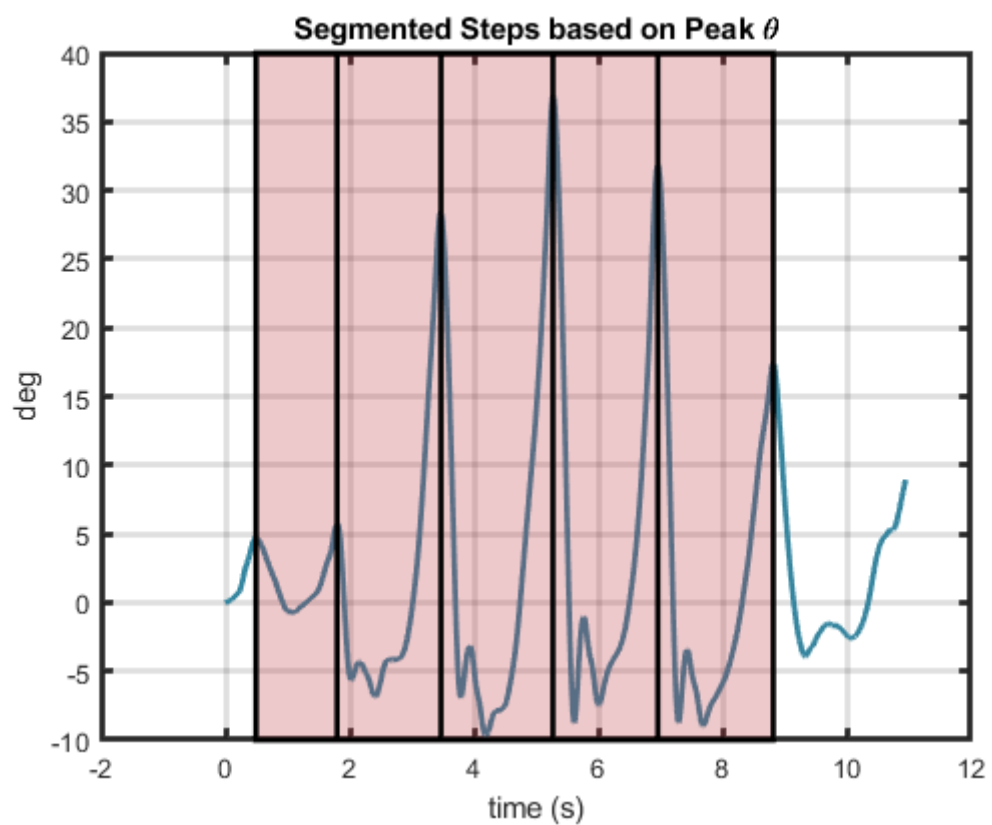


Figure 4.5: Step segmentation through peak angle detection

are set to zero. The wavelet coefficients are then reconstructed back into a signal. An example of DWT thresholding is shown in fig. 4.6. The reconstructed DWT acceleration data is used to detect foot-flat phase.

4.2.3.1 Finding Zero-Acceleration Points

Foot-flat phase is detected by looking for the zero regions in the anterior-posterior acceleration's derivative[81]. A threshold of $0.01m/s^2$ was set to account for small amounts of noise in the DWT signal. Acceleration points within this threshold were identified as zero-acceleration points. Zero-acceleration points less than 3-samples long are removed, since foot-flat phase is expected to be much longer. The end of foot-flat phase is estimated to be heel-off. An example of detecting stance phase is shown in fig. 4.7.

4.2.4 Zero Velocity / Zero Position Update

Zero-velocity and zero-position updates are used to reduce integration drift and improve the accuracy of the positional estimate of the tibia and SLL. The high-pass filtered vertical velocity signal is put through a low-pass 6th order Butterworth filter with a cutoff frequency of 6 Hz.

It is known that the vertical velocity during stance should be zero, but drift from integration will offset this value. Therefore, the vertical velocity at heel-off is set to 0, and the vertical velocity after heel-off is subtracted by the velocity reported at heel-off weighted based on the distance from the heel-off timepoint using the following formula [37]:

$$v'_{x,i} = v_{x,i} - v_{HO} * \frac{t_i - t_{TS}}{t_{HO} - t_{TS}}$$

Where at timestep i after heel-off:

- $v'_{x,i}$: corrected velocity
- $v_{x,i}$: original velocity
- t : time

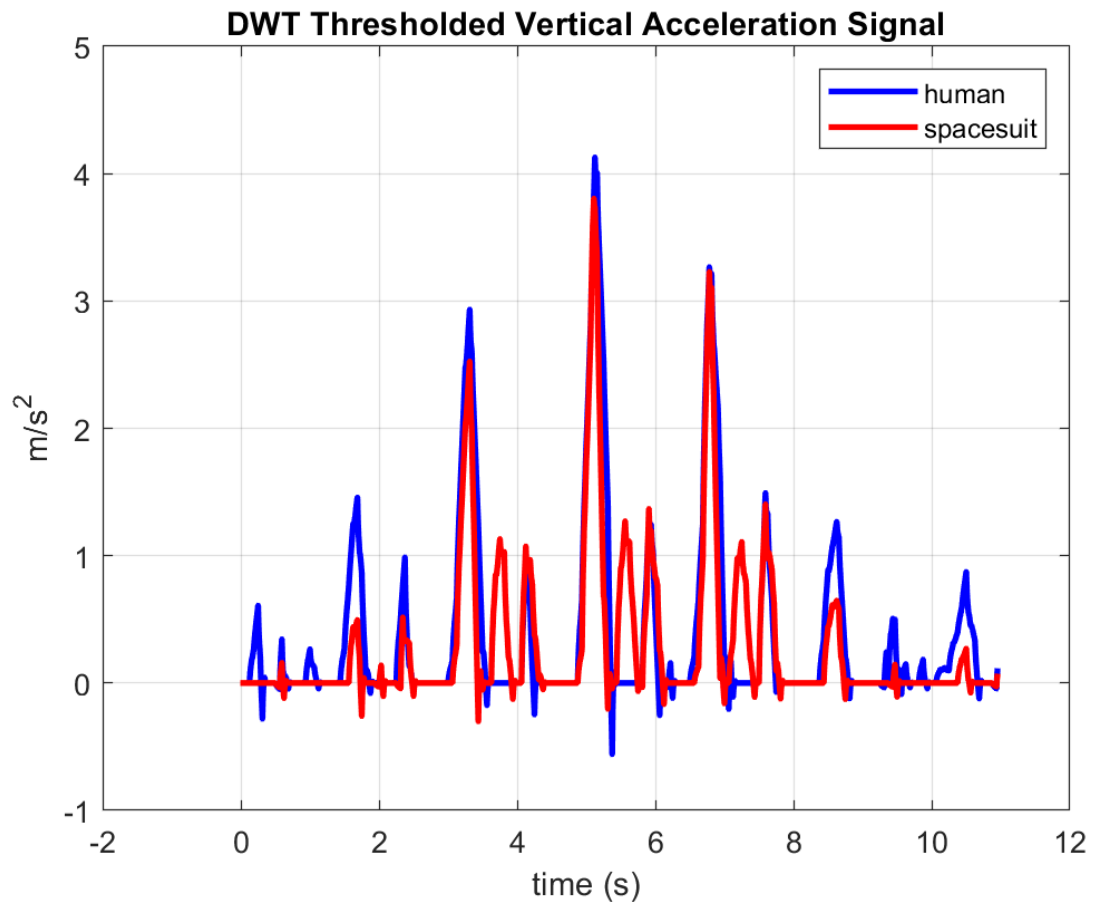


Figure 4.6: DWT transformed signal which was thresholded and then inverse transformed into the signal

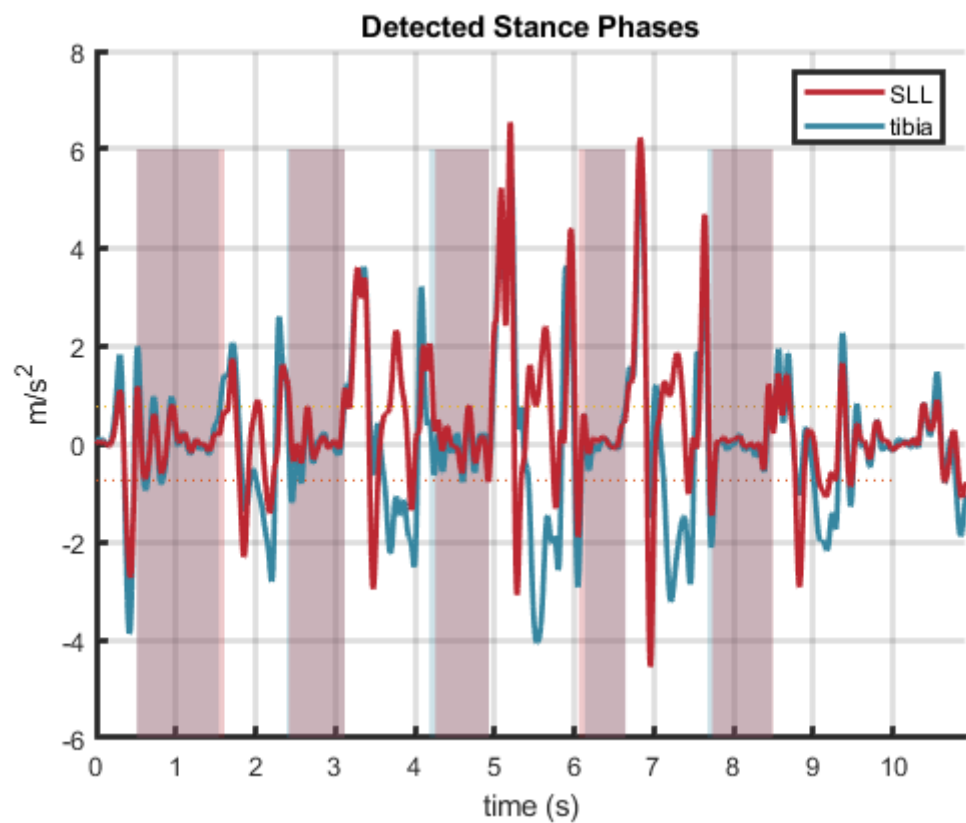


Figure 4.7: Stance phase detected by finding zero-acceleration points in each step

- TS : at next toe strike
- HO : at heel-off

To calculate the position of the tibia and SLL from heel-off, the integral of the corrected velocity is taken. Assuming the interface between the heel and boot is at point 0, taking the integral only from the estimate of heel-off acts as a zero-position update, under the assumption that just before heel-off, the heel and boot are flat on the ground. An example of the positional difference is shown in fig. 4.8

Since drift is not completely eliminated with the methods outlined, bounds need to be established where we can take the positional difference with confidence that the difference is not largely due to the drift.

While drift is not exactly a linear process, we made an assumption that finding the average drift value between two known points would be a reasonable approximation to quantify how drift accumulates over time in this scenario.

Analysis was conducted to determine the rate of drift after the ZVU/ZVP updates were performed. During stance phase, it's expected that both the SLL and tibia will have the same vertical position at toe-strike and heel-off. During swing phase, it is expected that both IMUs will return to the same vertical position after each step. Therefore, to calculate drift rate, the position values at the beginning and end of stance phase and swing phase were subtracted from each other, and then divided by the time of each phase, to get a drift rate. This rate represents the amount the IMU's positional estimate has drifted over each phase, when it is expected to return to 0.

IMU	Stance Phase Median Drift Rate	Swing Phase Median Drift Rate
Tibia	9.48 cm/s	14.15 cm/s
SLL	26.33 cm/s	27.48 cm/s

From this analysis, a limit of 0.04 s (1/26.33 cm/s) was used to take the positional difference between the SLL and tibia after heel-off, to measure heel-lift.

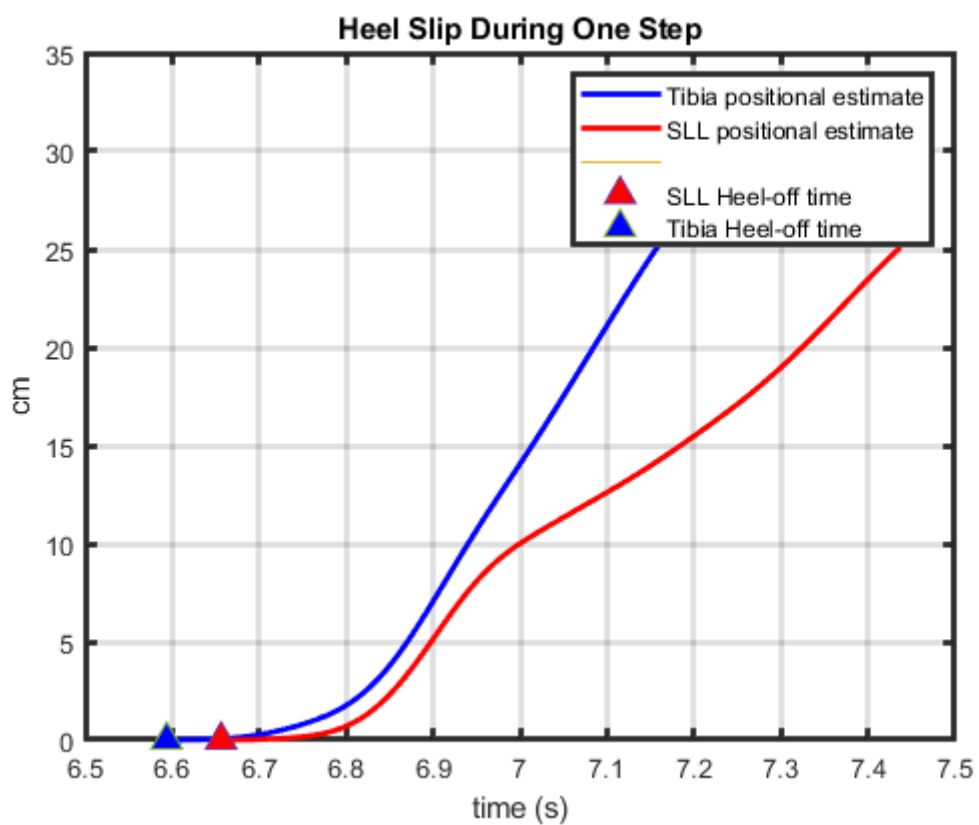


Figure 4.8: Heel lift measurement quantities between SLL and tibia IMUs

4.2.5 Outlier Step Removal

The heel-off detection was not perfect. In some cases, it failed to properly detect heel-off for the human or spacesuit with the parameters provided. Heel-off lag times $<-0.2\text{s}$ and $>0.2\text{s}$ were manually inspected, and if the detection times were incorrect, these steps were taken out of the analysis. A total of 32 steps were removed with this analysis.

For Subject 2, Configuration 2, the left tibia IMU dropped out. These steps were left out of the analysis.

For Subject 4, Configuration 0, Trials 1-12, the labels for the left and right IMUs seemed to be switched; the left SSL IMU was aligned with the right tibia IMU and vice-versa. Therefore, for these trials, the tibia IMU was switched to the other side. Since we don't know which IMU in particular was mislabeled, we don't know if the new labels are right for these trials. However, since we are not analyzing our data by sides, this data was left in the analysis.

4.3 Results

Heel-off lag is measured by subtracting the heel-off time of the tibia from the heel-off time of the SLL. However, since 0.04 seconds is a very small amount of time, it was decided to not record any heel-lift measures, as any heel-lift measurement would be minimal taken 0.04 seconds after heel-off. Measurements taken after this point may not be trustworthy due to the presence of accumulating drift. Therefore, heel-off lag was chosen as a proxy-representation of heel-lift; when there is lag in heel-off between the human and spacesuit, it is assumed to be accompanied by heel-lift.

Figure {fig. 4.9} shows the distribution of heel-off lag measurements in violin plots. It seems that subject 4 is the only subject to experience a “negative” heel-off lag. Subjects 2 and 3 experience only “positive” heel-off lag, which would suggest that these subjects experienced heel-lift.

“Negative” heel-off lag is technically impossible: when the spacesuit experiences heel-off, it will also push on the human-heel, causing it to experience heel-off as well. Another explanation for

this vertical acceleration is spacesuit leg lengthening, where during foot-flat phase, the spacesuit lower leg slowly expands in the anterior-posterior direction, causing the mounted IMU to register a positive acceleration. This may be due to interactions at the knee joint or from femur movement.

For subject 4, it is difficult to say whether they experienced heel-lift, since the distribution of lag seems to be centered around 0. Since Subject 4 has the largest crotch height, knee height, hip breadth, and thigh circumference, they may have some interaction within the lower torso to cause SLL leg lengthening.

Figures {fig. 4.10; fig. 4.11} show example zoomed-in views of the foot-flat phase for the DWT acceleration signal. Foot-flat is where both the blue (human) and red (spacesuit) lines are flat, and are shaded with the respective colors for the spacesuit and human.

In {fig. 4.10}, the spacesuit has some vertical acceleration before the human, suggesting that it may experience heel-off before the human does inside the spacesuit.

{fig. 4.11} shows an example where the human has some vertical acceleration before the spacesuit, which may suggest that they experienced heel-lift. As the human lifts their leg to initiate movement, the spacesuit does not respond and therefore does not experience heel-off at the same time, leading to heel-lift.

4.4 Summary

Presence of heel-lift was able to be detected by the methodology outlined in this specific aim, however it was unable to be reliably quantified due to the short confidence bounds from which a measurement can be taken. Heel-lift was detected for Subjects 2 and 3, but there was no noticeable effect of padding on heel-lift presence. Subject 4 seemed to be experiencing suit pressurization effects lengthening the lower leg during heel-off. This may be due to their larger lower-torso anthropometry. Fineman et al [39] suggested that relative coordination of the lower-torso may be affected by boot fit issues. However, results from this analysis suggest that boot-fit issues may be due to mismatch of lower-torso fit, and reiterate the importance of the kinematic chain in providing mobility. While this study was not able to quantify the amount of heel-lift, it

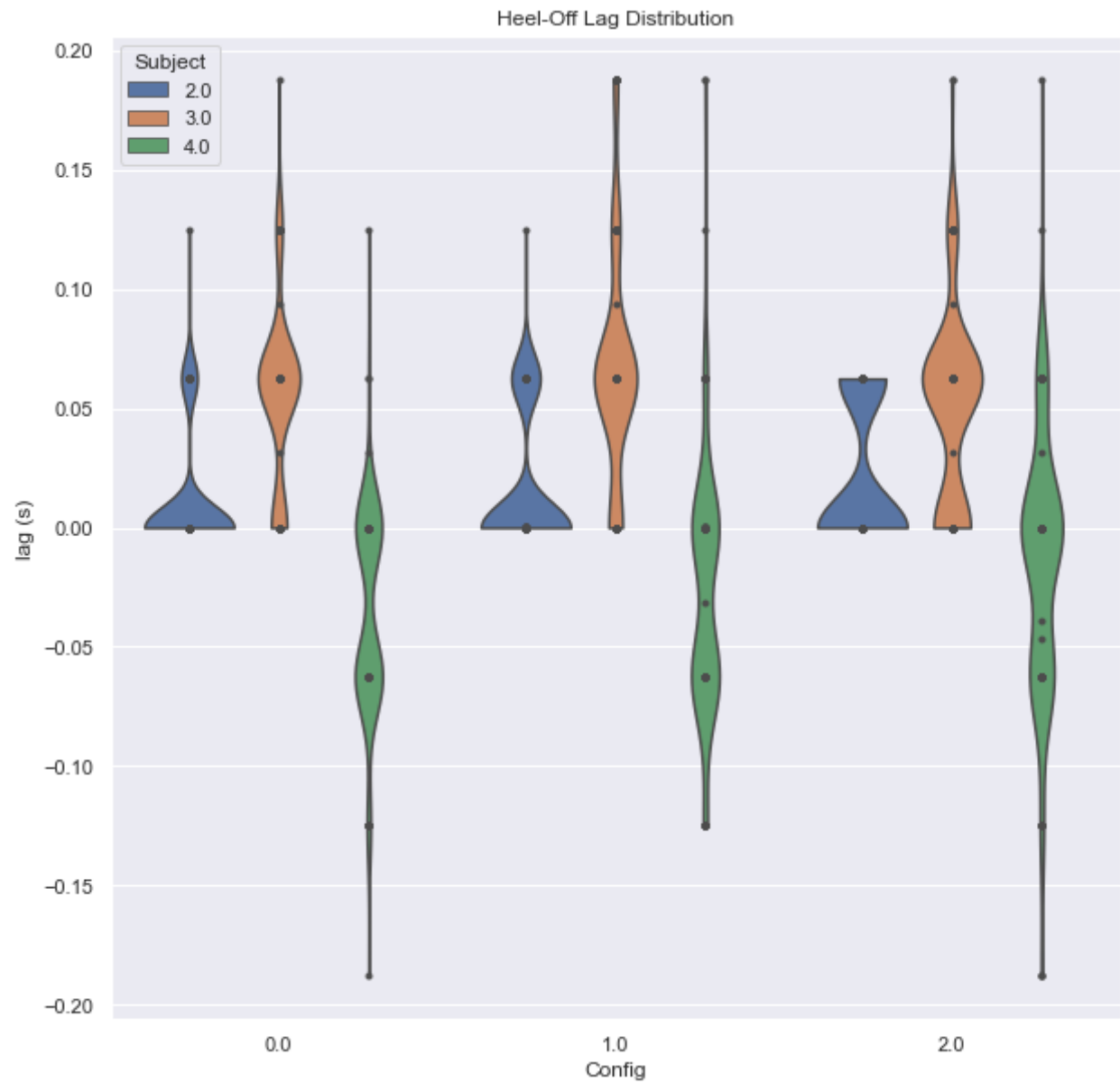


Figure 4.9: Heel-off lag distributions between all subjects and configurations

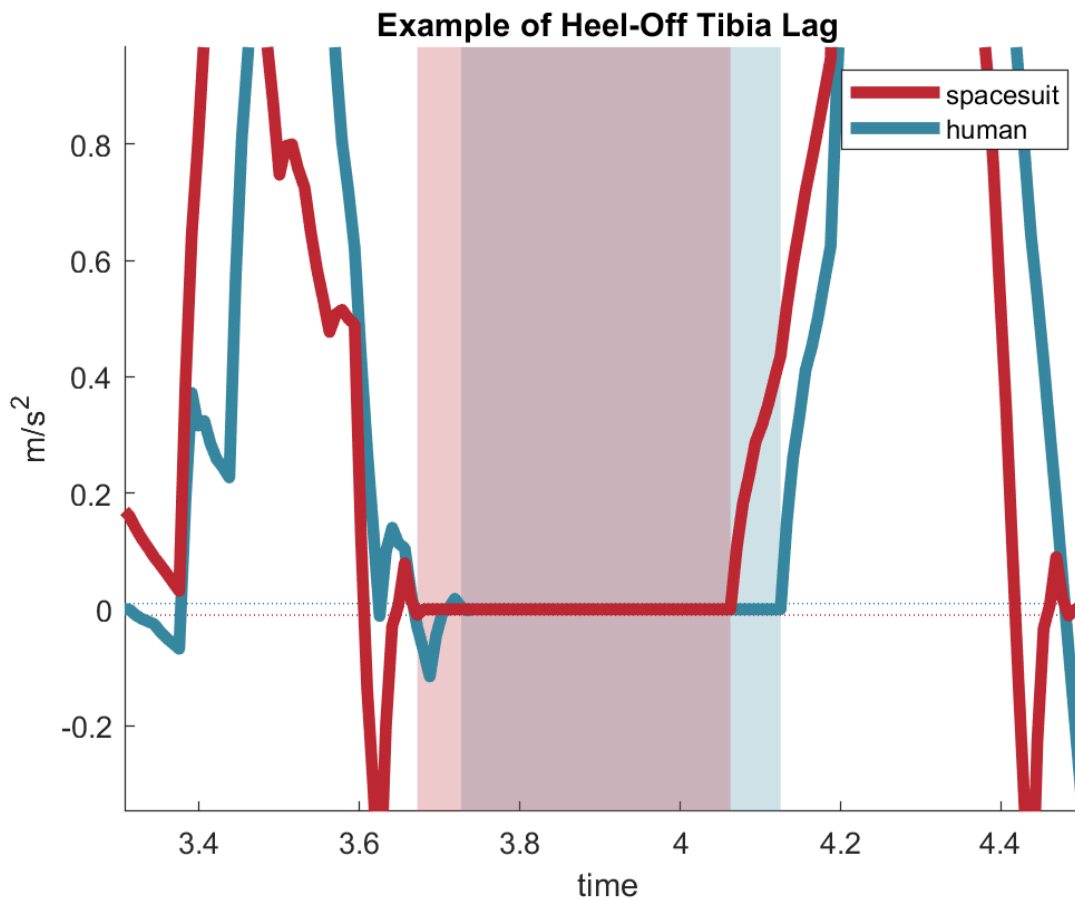


Figure 4.10: DWT transformed SSL and tibia vertical acceleration. The shaded regions represent the detected stance phases, with the right-most shaded portion being heel-off. As seen here, the SSL experiences a vertical acceleration before the tibia, causing “negative lag”

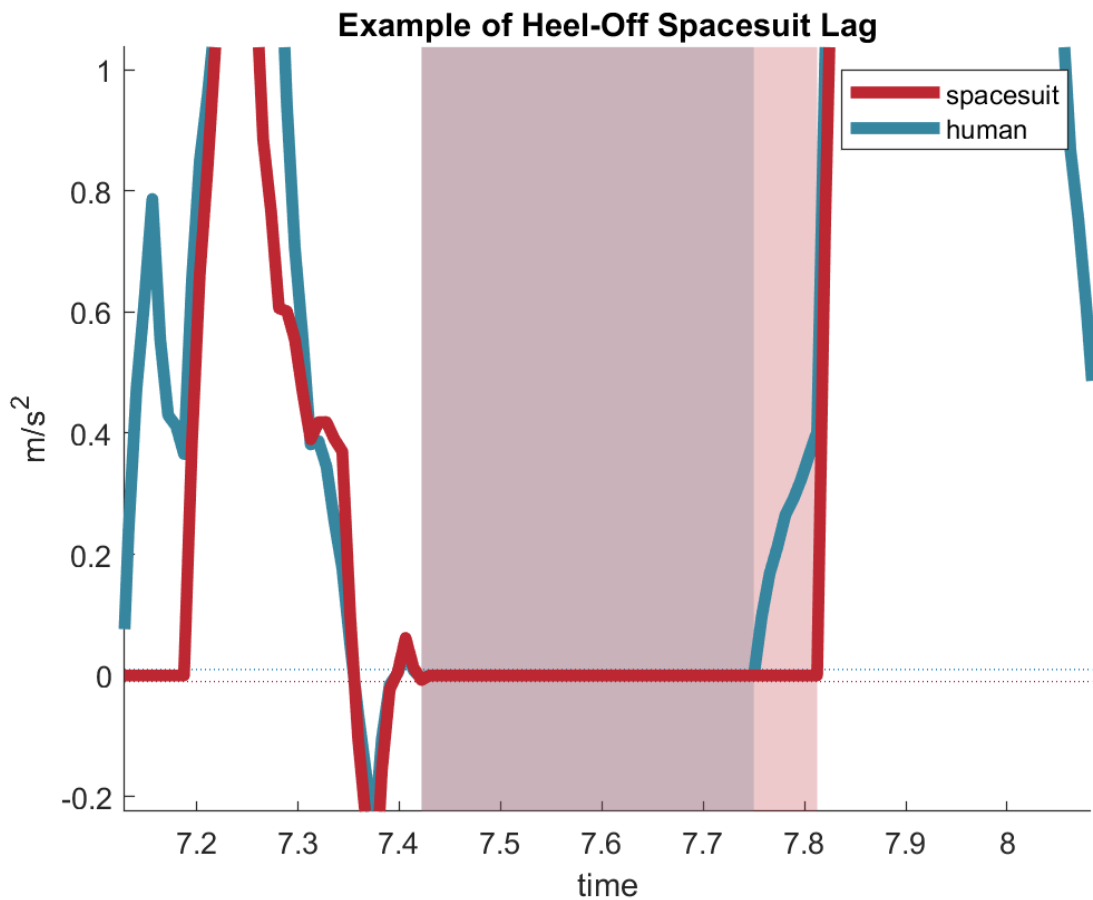


Figure 4.11: DWT transformed SSL and tibia vertical acceleration. The shaded regions represent the detected stance phases, with the right-most shaded portion being heel-off. As seen here, the tibia experiences a vertical acceleration before the SSL, which may lead to heel-lift

does present a new method to detect heel-lift by using biomechanics analysis techniques. These techniques have been validated for non-suited applications, but future work may try to validate these techniques for suited applications with the addition of a contact sensor below the heel to detect heel-lift.

Currently, all analysis is complete with this work. This work is currently in preparation as a technical note to be submitted for peer-review.

Chapter 5

Specific Aim 2: Predictively modeling dynamic changes in foot morphology during gait

5.1 Introduction

Foot shape is known to be highly variable throughout the population, including by sex [130, 71, 72], age [123], and weight [101]. This variability is often not captured in footwear sizing, as current footwear fitting standards only use foot length, foot width, and arch length to fit to standardized shoe sizes [8]. Furthermore, footwear is commonly designed around lasts, shoe molds that are sized and shaped by each manufacturer with no common standard, leading to variability in footwear shapes and sizes [59, 126]. Such variability can make it hard for consumers to find a proper fit, resulting in users having to wear ill-fitting footwear with suboptimal comfort [31]. Footwear comfort has shown benefits in increasing running performance [75] and reducing the risk of movement-related injury [86], and is often the number one [82] factor for consumers to select footwear. Footwear should therefore be properly fit to a wide population range in order to be successful.

However, because the current methodology of designing footwear relies on using static lasts, this assumes that the foot consists of rigid segments. This fails to account for dynamic changes in foot morphology, especially when the foot is being loaded during gait. Assumptions of rigid foot segments during foot loading have shown inaccuracies in estimation of ankle joint mechanics [133, 63], suggesting intra-foot motion as the foot is loaded [74, 129]. Evidence suggests that foot loading affects linear foot measurements, such as when transitioning from sitting to standing

[131, 93] or during the stance phase of gait [69, 9, 50]. The dynamically changing measurements suggest morphological changes occurring, all of which may not be captured in static linear and circumferential measurements. Thus, it becomes difficult to characterize the wide variety of foot shapes across not only a large population, but within individuals as their foot goes through loading scenarios such as gait.

Statistical shape models (SSMs) can explain morphological differences across populations by identifying shape modes which account for variance from the mean foot,. These have been developed for whole-body digital human modeling applications to study population and individual variance in body shape [3, 6, 104, 96, 97]. Parametric SSMs are extensions which use correlations between subject anthropometric data and SSM deformations to help predict body shape for new individuals in the population [96, 97].

SSMs have recently been applied to characterize static foot shape across a population [28] and recognize foot-shape deviations [117]. The aforementioned efforts to capture foot measurement changes over the gait cycle did capture 4D foot images [9, 50], but these efforts were not translated into a SSM. All the previously developed systems were also based on a catwalk, requiring subjects to correctly hit the scanning area for a successful data capture, which may not be representative of natural cadence. However, the systems used to capture 4D foot shape are very expensive and cannot be used around a treadmill, which allows for subjects to fall into natural gait. No SSMs have been developed to predict dynamic foot shape from previous capture of 4D foot scans.

Therefore, the objectives of this specific aim are: - develop a low-cost 4D scanning system capable of capturing foot shape around a treadmill - create a predictive model of foot shape changes across the dorsal surface during stance phase - identify specific areas of the foot that change shape during stance phase - correlate changes in foot shape across large-scale population foot measurements

This chapter is split into two sections, the first outlining development of the 4D scanning system, and the second detailing construction and analysis of the model.

5.2 DynaMo: Dynamic Body Shape Capture with Intel RealSense Cameras

5.2.1 Background

Human body shape can be captured with a variety of methodologies, including laser lines, structured light, photogrammetry, and millimeter waves [?]. However, these technologies require expensive modules and have limited ability to capture dynamic changes in body shape.

Motion capture with specific markers is commonly done through camera-based motion tracking [?] These systems for marker tracking are often cost prohibitive and unable to capture surface morphology.

Recently, Intel released the D415 and D435 RealSense Depth Cameras, which use near-infrared structured light patterns and two infrared imagers to capture depth information at up to 90 frames per second. Purchasing a set of these cameras is more affordable than buying a dedicated motion-capture system for shape or marker tracking.

While Intel provides the `librealsense` library to interface with their cameras, it lacks tools to use multiple devices at once to capture shape and marker-tracking information. DynaMo builds upon `librealsense` to provide additional capability for researchers looking to capture such data.

DynaMo is designed to primarily assist those in the biomechanics and medical fields in capturing motion or body-shape data. It is currently being used in the Anderson Bioastronautics Research Group to capture dynamic changes in foot morphology.

5.2.2 Methods

DynaMo is a Python library that provides tools to capture dynamic changes in body shape and track locations of markers using Intel RealSense D4XX cameras. DynaMo was developed from the examples provided by Intel in the Python `librealsense` library. It has been successfully tested streaming six cameras at 90 frames per second, all connected to one computer. DynaMo consists of several scripts that allow for calibration of multiple RealSense D4XX cameras to a common global coordinate system, simultaneous streaming of multiple RealSense D4XX cameras, viewing of

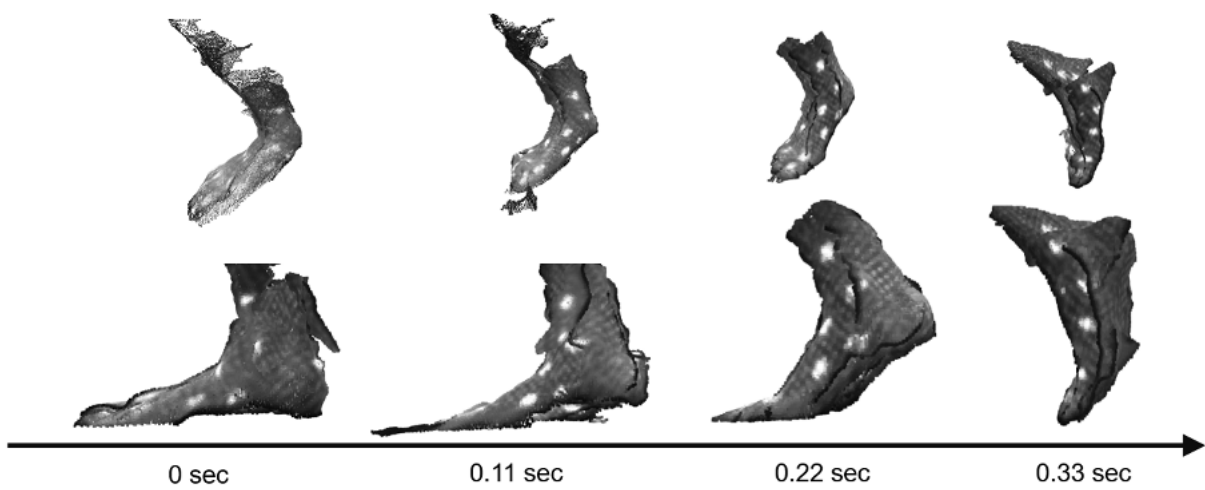


Figure 5.1: Sample frames collected by DynaMo showing dynamic shape capture

data from multiple RealSense D4XX cameras in pointcloud format, and identification of reflecting markers from the pointclouds. The library is optimized to reduce the number of dropped frames while streaming.

DynaMo allows for the capture of depth, infrared, and color frames at an $(u \times v)$ resolution from Intel RealSense cameras. The values that are captured in each frame are listed below:

- Depth frames: s , where s is the distance to the object
- Infrared frames: Y , where Y is a single value from 0-255 denoting the monochrome pixel value
- Color frames: $[R, G, B]$, where R, G, B are red, green, and blue values, stacked to represent the color value of the pixel. This results in a $(u \times v \times 3)$ dimensional frame.

The pinhole camera model [?] projects 3D points from the world $[x, y, z]$ onto a 2D image plane $[u, v]$ using the following formula:

$$s \begin{bmatrix} u \\ v \\ 1 \end{bmatrix} = K \times \begin{bmatrix} x \\ y \\ z \end{bmatrix}$$

Where K is a matrix describing the camera's intrinsic properties, and s is the distance between the real-world point and the image plane. These properties include the focal length (f_x and f_y) and image offset (pp_x and pp_y) in each direction. They are represented in the matrix as:

$$K = \begin{bmatrix} f_x & 0 & pp_x \\ 0 & f_y & pp_y \\ 0 & 0 & 1 \end{bmatrix}$$

Since we are collecting 2D frames and we want to know the 3D location of the point to reconstruct the pointcloud, we can simply invert the K matrix and solve for the $[x, y, z]$ location as we know s , the distance between the 3D point and the 2D plane, and $[u, v]$, the coordinate of the point in the 2D plane:

$$\begin{bmatrix} x \\ y \\ z \end{bmatrix} = \begin{bmatrix} \frac{1}{f_x} & 0 & \frac{-pp_x}{f_x} \\ 0 & \frac{1}{f_y} & \frac{-pp_y}{f_y} \\ 0 & 0 & 1 \end{bmatrix} \begin{bmatrix} s * u \\ s * v \\ s \end{bmatrix}$$

This transformation is known in the computer vision community, and is crucial to the functions present in **DynaMo**. **DynaMo** uses this transformation extensively in its calibration, streaming, and marker-tracking features.

Connected cameras are setup using a `device_manager` object which handles calls for communicating with the cameras. Cameras are first calibrated to a common global coordinate system by using a defined chessboard viewable by all cameras. The chessboard points are detected using the `findChessboardCorners` function of the OpenCV library [17] for each camera's color image. Once the chessboard corners are found, they are translated to 3D points from the perspective of each camera and centered.

The Kabsch algorithm [61] is used to compute the (3×3) rotation matrix between each camera and the known chessboard coordinates. Translation is calculated by taking the difference between the known chessboard corners and the camera's rotated chessboard perspective, resulting in a (3×1) matrix. The rotation matrix is horizontally stacked to the translation matrix, and a row of $[0, 0, 0, 1]$ is added to create a (4×4) matrix. This matrix transforms each camera's pointcloud from its local coordinate system to a global coordinate system.

Streaming is achieved by reading frames from each camera into a dictionary object saved in the computer's RAM. **DynaMo** checks frame numbers for continuity to ensure that frames are collected synchronously and are not repeated. Once streaming is complete, **DynaMo** aligns the images collected by the sensors in each camera to a common image center and saves the images as `pickle` objects to the disk. The data from all cameras can then be viewed as a single pointcloud for each frame from all cameras by using the previously computed transformation matrix.

5.3 Development of a Predictive Dynamic Foot Shape Model from Statistical Shape Modeling

The development of the DynaMo software [15] for the Intel RealSense D415 Depth Cameras (Intel, Santa Clara CA) allowed a 4D scanning system to be set around a treadmill, where subjects can maintain a natural cadence. This system captures the majority of the foot's dorsal surface, but does not allow for the capture of the foot's plantar surface. 4D scans are captured at 90 fps, enabling a detailed evaluation of foot morphology changes during loading and unloading. This section outlines the development of a parametric SSM, derived from scans captured with this system. The parametric SSM can characterize and predict dynamic foot morphology at specific points during stance phase across the subject population.

5.3.1 Methods

5.3.1.1 Subjects

A total of 30 healthy subjects (15 men and 15 women, ages 23.1 ± 3.7) participated in this study. Subjects were recruited in a stratified sample into one of six groups (5 subjects per group) to maximize variance in population foot length. Height was used as the grouping factor since height is well correlated to foot length [46]. The general population may not know offhand their exact foot length, and shoe size varies by manufacturer and does not correspond directly to foot length [59, 126]. Groups consisted of 5th-35th, 35th-65th, and 65th-95th height percentiles for each sex. Height percentile values were taken from the ANSUR II survey [47] and converted to imperial units as it was expected most subjects would report their height in imperial units. Population recruitment groups are summarized in *tbl. 5.1*.

Table 5.1: Enrollment groups based on reported height. 5 subjects were enrolled in each group

Sex	5th-35th percentile Height	35th-65th percentile Height	65th-95th percentile Height
Female	4'11"-5'3"	5'3"-5'5"	5'5"-5'8"
Male	5'4"-5'8"	5'8"-5'11"	5'11"-6'2"

Prior to recruitment, subjects completed a prescreening survey to ensure they were adequately healthy by the American College of Sports Medicine guidelines[106], and between the ages of 18-65. Subjects provided their sex and height, and were only enrolled in the study if their population group was not fully enrolled.

5.3.1.2 Experimental Procedures

The experimental protocol was approved by the University of Colorado Institutional Review Board. Procedures were explained to each subject and written consent was obtained prior to participation. Subjects' height and weight were recorded with a tape measure and scale, respectively. Subjects' foot length, foot width, and arch length were measured with a Brannock device (The Brannock Device Company, Liverpool, NY) [8]. Both foot length and arch length were measured in centimeters. Foot width was measured as an ordinal size (e.g. A, B, C, D, E), and then converted to a linear measurement in centimeters (The Brannock Device Company, Liverpool, NY).

Six Intel RealSense D415 Depth Cameras (Intel, Santa Clara, CA) were placed and calibrated around a custom-built level treadmill in the University of Colorado Boulder Locomotion Laboratory, as shown in fig. 5.2. The DynaMo software package was used to capture depth images of the right foot at 90 frames-per-second while subjects walked on the treadmill, and convert each frame's depth images to a single point cloud [15].

The treadmill was set to an average walking pace of 1.4 m/s [18]. Reflective markers were placed on the subject's right foot and a black sock over their left foot to aid in right foot iden-

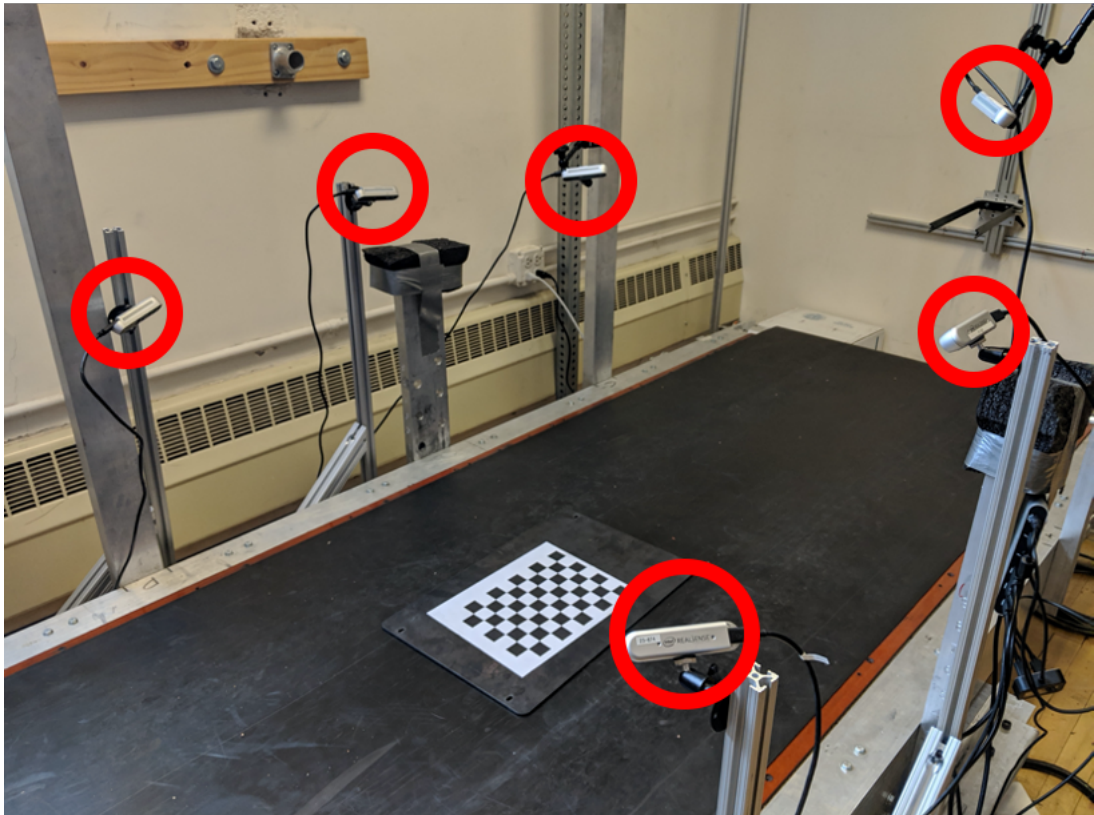


Figure 5.2: Capture setup of 6 Intel RealSense D415 Depth Cameras (circled in red) placed around a treadmill. The checkerboard shown was used to calibrate the cameras using the DynaMo package.

tification. Subjects first walked for one minute to warm-up and fall into a natural cadence. The operator then collected 10 seconds of data to capture approximately 10 steps. The data were reviewed to ensure the subject stayed in frame from heel-strike to toe-off during capture. If needed, the subject's placement was shifted and data was collected again, up to two times.

5.3.1.3 Data Processing

(Fig. 5.3) provides an overview of the data processing workflow.

5.3.1.4 Mesh Construction

For each subject, a candidate heel-strike to toe-off event was manually identified across all captures by taking into account point cloud quality due to the high computational power required to process all heel-strike to toe-off events. The depth images captured by each depth camera were processed into point clouds using the DynaMo package [15]. The C++ implementation of the PointCloud Library [108] was used to identify and isolate the right foot from the point set. First, the point clouds were downsampled with a voxel size of 3 mm to reduce required computing power. A RANSAC algorithm [42] was used to identify the flat treadmill floor with a plane model, and remove it from the point cloud. Euclidean cluster extraction was then used to detect the point clusters that make up each foot. The total color value of each point cluster was used to identify the right foot from the left foot, as the left foot had a lower total color value due to the black sock. The left foot was then removed from the point cloud, leaving only the right foot for processing.

Poisson surface reconstruction was done using Open3D [135]; this adds a topological layer interpreted from the pointcloud. Point normals were calculated for the point cloud using the 10 nearest neighbors. A ball-pivoting algorithm [12] is then used with the point normals to estimate the surface from the point cloud and construct the foot scan mesh.

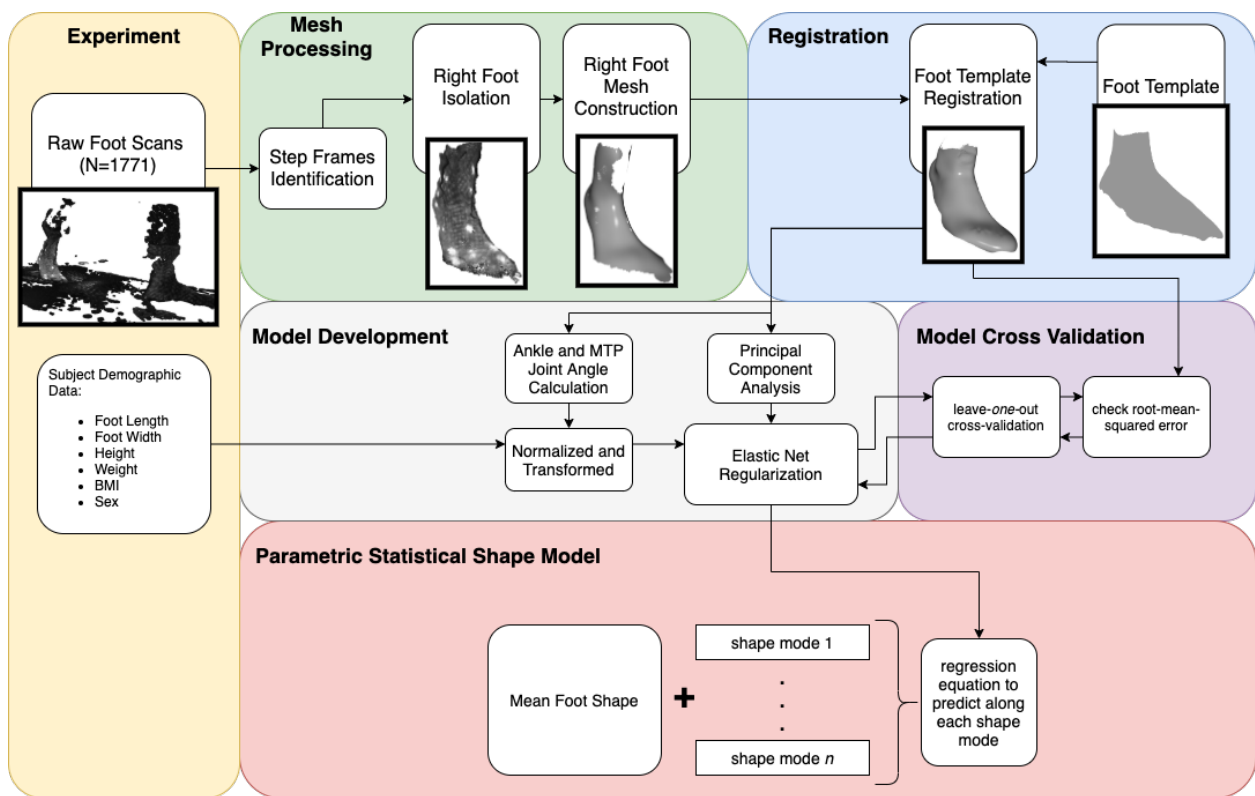


Figure 5.3: Flowchart of processing steps for statistical shape model creation

5.3.1.5 Foot Template Registration

From the provided template, the toes were smoothed into a single structure and parts of the upper shank removed to be better fit to the captured data, with a finalized structure of 29873 points. The overall registration process follows a three-step process: a rough alignment followed by two radial-basis function (RBF) fine alignment steps

The registration process was first completed for each subject's data with a foot scan mesh manually identified near mid-stance. A point-to-plane iterative-closest-point (ICP) algorithm [27] was used to roughly align the template foot to the scan mesh with the Open3D library [135].

Corresponding points between both the scan mesh and the ICP-aligned template were found using a radial-search KD-Tree implemented in the Open3D library [135]. Any points on the scan mesh which were not within 1 cm of a corresponding point on the aligned template were deleted; these points represented parts of the treadmill floor which were missed in the RANSAC identification and parts of the upper shank. Similarly, any points on the template not within 1cm of a corresponding point on the scan mesh were temporarily set aside from the template; these points correspond to those near holes in the scan mesh which would be refilled in later processing

Thin-plate spline RBFs have been used to surface fit templates to scanned body shapes [96], and so were used in two stages in this research. A first-pass RBF registration, using a thin-plate spline for interpolation, was done between the template and the scan using the GIAS2 package [134]. To prevent overfitting of the RBF to the noise on the edges of the captured pointcloud, a maximum of five iterations were done on the first-pass RBF registration process. The first-pass registered RBF template was then appended with the points previously removed from the template. This intermediate template represents the template fitted to the known scan data, with any unknown sections (e.g. holes in the scan data), taking the value of the template. However, the disparity between the known and unknown sections created major discrepancies in the morphed template not representative of the scan data.

A second-pass RBF registration was done from the ICP-aligned template to the intermediate

template with the same parameters as the first-pass registration. This smooths out the unknown sections representing holes in the scan data with the surrounding known sections. The second-pass registered template was saved as the final registered template.

Following the registration of the mid-stance scan, the process was repeated both forwards towards toe-off and backwards toward heel-strike on a scan-by-scan basis. In this iterative fashion, the previous scan's registered template was used as the template for the following scan. During the iterative registration process, the RBF alignment was only conducted for one iteration for both the first-pass and second-pass to prevent over-fitting.

5.3.1.6 Joint Angle Calculation

The original template identified the lateral malleolus, medial malleolus, 1st metatarsal head, 5th metatarsal head, and 2nd toe landmarks as certain vertices. New landmark vertices for the lateral shank and medial shank were manually picked on the template.

Post-registration scans were aligned to a common coordinate frame based around the toes. The origin was defined as the point along the vector from the 1st metatarsal head landmark to the 5th metatarsal head landmark which is orthogonal to the second phalange. From the origin, the x-axis, was defined as pointing towards the 2nd toe. The y-axis, was pointed towards the 5th metatarsal. The z-axis was the cross-product of both x- and y-axes, pointed upward. This coordinate system also served as the static coordinate system for the MTP joint.

The ankle joint center was defined as the midpoint between the medial and lateral malleous. The ankle's local z-axis is aligned vertically with the shank center, defined as the center between the lateral shank and medial shank landmarks. The ankle's local y-axis is aligned from the shank center to the lateral malleolus. The ankle's x-axis is the cross-product of the y- and z-axis, pointed in the forward direction towards the toes.

Static reference angles were taken from these coordinate systems at mid-stance. For the ankle joint, the z-axis served as the internal/external rotation axis, the y-axis as the dorsi/plantarflexion axis, and the x-axis as the inversion/eversion axis. Since the model's origin was at the toes, the

calculation for MTP dorsi/plantarflexion was modified. The new local MTP joint coordinate system had the x-axis defined as pointing from the ankle joint center to the MTP joint center, as such the y-axis represented MTP dorsi/plantarflexion. Since there is little flexibility in the transverse and frontal planes of the MTP joint, the x-axis therefore represented whole foot inversion/eversion, and the z-axis represented whole foot internal/external rotation around the origin. MTP and ankle joint angles were calculated for every other scan as the Euler angle difference from the static joint coordinate system around each axis. Each subject's joint angles are low-pass filtered with a 2nd order low-pass Butterworth filter with a cutoff frequency of 15 Hz. The global and local coordinate systems are summarized in fig. 5.4.

5.3.1.7 Model Construction

Principal component (PC) analysis is a dimensionality-reduction method commonly in constructing SSMs [103, 96, 28, 117]. The first PC represents an axis containing the largest variance in the dataset, and each subsequent PC describes the largest variance orthogonal to the previous component's axis. Therefore, PCs allow for a new, smaller set of orthogonal variables to be defined which represent the variance in the dataset.

Let N equal the number of total scans in the dataset, and $n = 29873$ equal the number of vertices in each registered scan. The scikit-learn module [99] was used to incrementally calculate the maximum N PCs which represent the dataset. Each scan in the dataset is represented in the PC model with N PC scores. All PC scores are centered around 0, which represents the mean foot scan of the dataset containing all subjects. Each PC represents a shape mode in the SSM, where each score represents a deviation from the mean foot along the shape mode axis. The resultant PC model can be used to inverse transform a vector of length N PC scores into a 29873×3 vector, which represents the location of the vertices in the foot shape. Not all PCs were retained in the model since the first few PCs explain a majority of the variance, while additional PCs may be accounting for noise.

Subject demographic data and calculated joint angles were incorporated into the SSM by

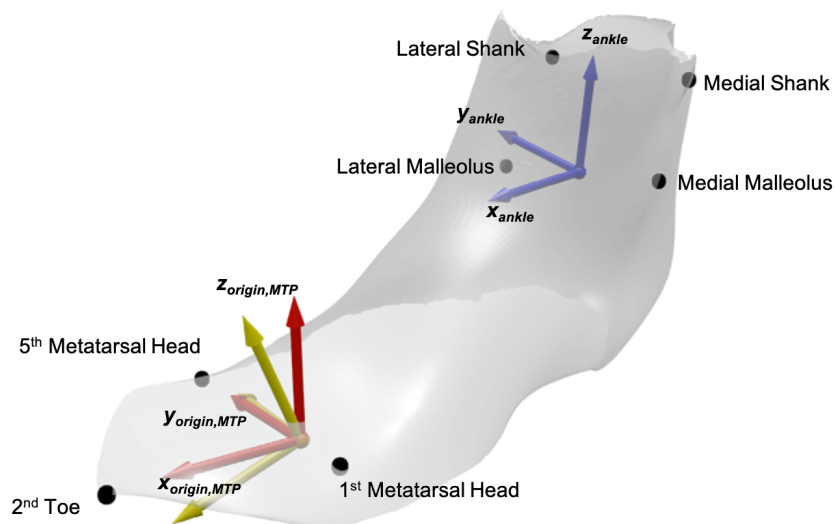


Figure 5.4: Coordinate system defined from registered scans. Anatomical landmarks are shown as black dots. The ankle joint's local coordinate system is shown in blue, the MTP joint's local coordinate system is shown in yellow, and the model's origin coordinate system is shown in red. Directions for each coordinate system are shown in bold text

developing multivariate linear regression models based on these features. This was used to predict each PC score, which can then be inverse-transformed into a foot shape. Subject demographic data and joint angles were normalized and power-transformed to aid in regression development [132]. An elastic net regularization algorithm [136] was run for each multivariate regression to calculate normalized feature coefficients for each PC score's regression. Two different sets of predictors were created, one with all subject demographic data and calculated joint angles, and one with the highly cross-correlated predictors of arch length, body-mass index, and height were removed (see Supplementary Figures). Six potential models were built as combinations between the number of PCs predicted which explained 95%, 98%, and 99.7% of the variance, and the two predictor sets.

5.3.1.8 Model Validation

All six models were validated for performance using leave-one-out cross-validation, where scans from each subject were set as the validation set, and models were trained on the remaining dataset. Model performance during validation was quantified with the root mean squared error (RMSE) of the predicted foot shape to the corresponding registered scan. A two-way RMANOVA analysis was run on the error distributions to test the effect of constructing a predictor with the different number of PCs, and between using the two variable sets. The chosen model was retrained on the whole dataset before being analyzed.

5.3.2 Results

A total of 1771 scans were analyzed across all 30 subjects. Each subject's stance phase ranged from 52-69 scans (mean=59). (Fig. 5.5) shows a set of raw and registered scans from one subject. All processed scans were registered to the template with a median registration accuracy of 1.0 ± 0.6 mm.

The PCA analysis of all registered scans found the first 8 PCs to represent approximately 95% of the variance, the first 27 PCs to represent approximately 98% of the variance, and the first 105 PCs to represent approximately 99.7% of the variance. (Fig. 5.6) shows the distribution of

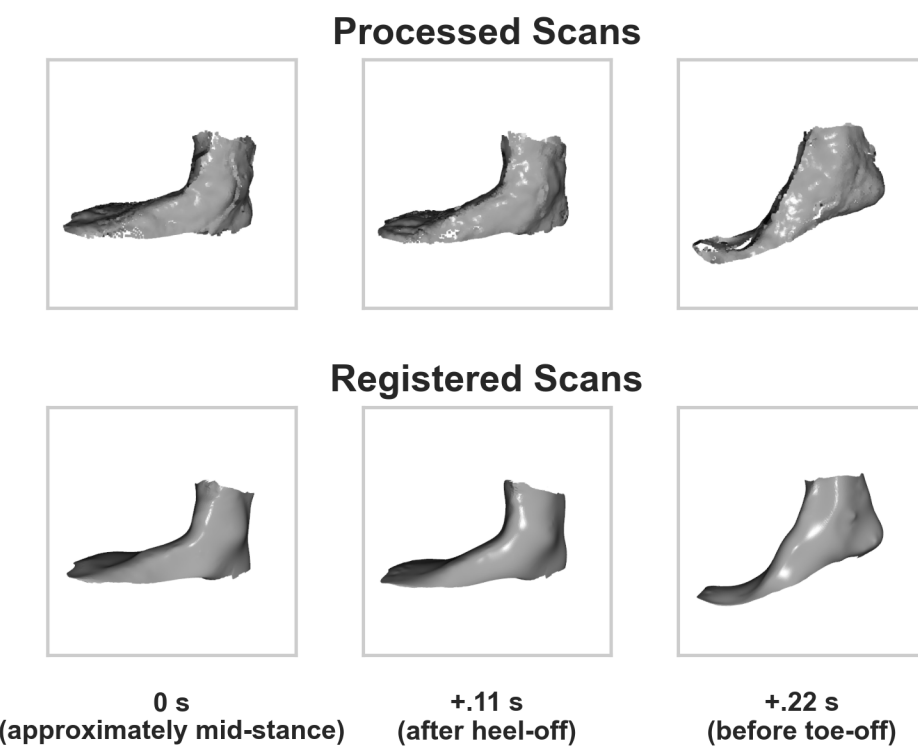


Figure 5.5: Processed and registered scans of one subject during heel-off, shown 10 frames (.11 seconds) apart

cross-validation RMSEs for each of the six elastic net regression models tested. RMSE distributions did not meet assumptions for normality, but RMANOVA was still used to compare models due to its resiliency to deviations from normality. A significant difference was found between predicting different numbers of PCs ($F=1595.0$, $p<0.001$), predicting between the two variable sets ($F=81.6$, $p<0.001$), and the interaction between both factors ($F=213.7$, $p<0.001$). Significant differences were found between all three levels of the predicted number of PCs ($p\text{-adj}<0.001$) with a Tukey post-hoc HSD test. No significant difference was found between the two variable sets ($p\text{-adj}=0.42$). Therefore, the model predicting 8 PCs with the selected variable set was chosen for its simplicity and performance.

Each retained PC is a shape mode in the model. (Fig. 5.7) shows the chosen model's normalized regression coefficient values for each shape mode. The coefficients for the sex predictor are not shown as they were calculated to be zero for every shape mode.

(Fig. 5.8) shows each shape mode's axis represented on the mean foot, highlighting which areas of the foot are affected by deformations in each shape mode. (Fig. 5.9) shows the ± 2 standard deviations of deformation along each shape mode overlaid on the mean foot. Supplementary information includes correlation between figures, ratio of total variance each retained PC accounts for, and a video showing the predictive capability of the model.

This study was designed to construct and evaluate a parametric SSM in explaining and predicting dynamic foot morphology changes across the subject population. The model was able to predict dynamic foot shape across the subject population with an average RMSE of 5.2 ± 2.0 mm. For context, if all possible prediction error was accumulated to only affect length and width, it would be higher than the half-size step of the American shoe sizing system [77], but less than inter-brand variability of shoe length and shoe width [126]. Further, this error is lower than the RMSEs of other parametric SSMs that predicted static standing child body shape (mean=10.4mm) [96], dynamic shoulder deformation (mean=11.98mm) [65] and child torso shape (mean=9.5mm) [97]. Note though, that the presented model may have lower prediction errors due to the foot being a relatively smaller section of the body to model. Grant et al's model reconstructed internal

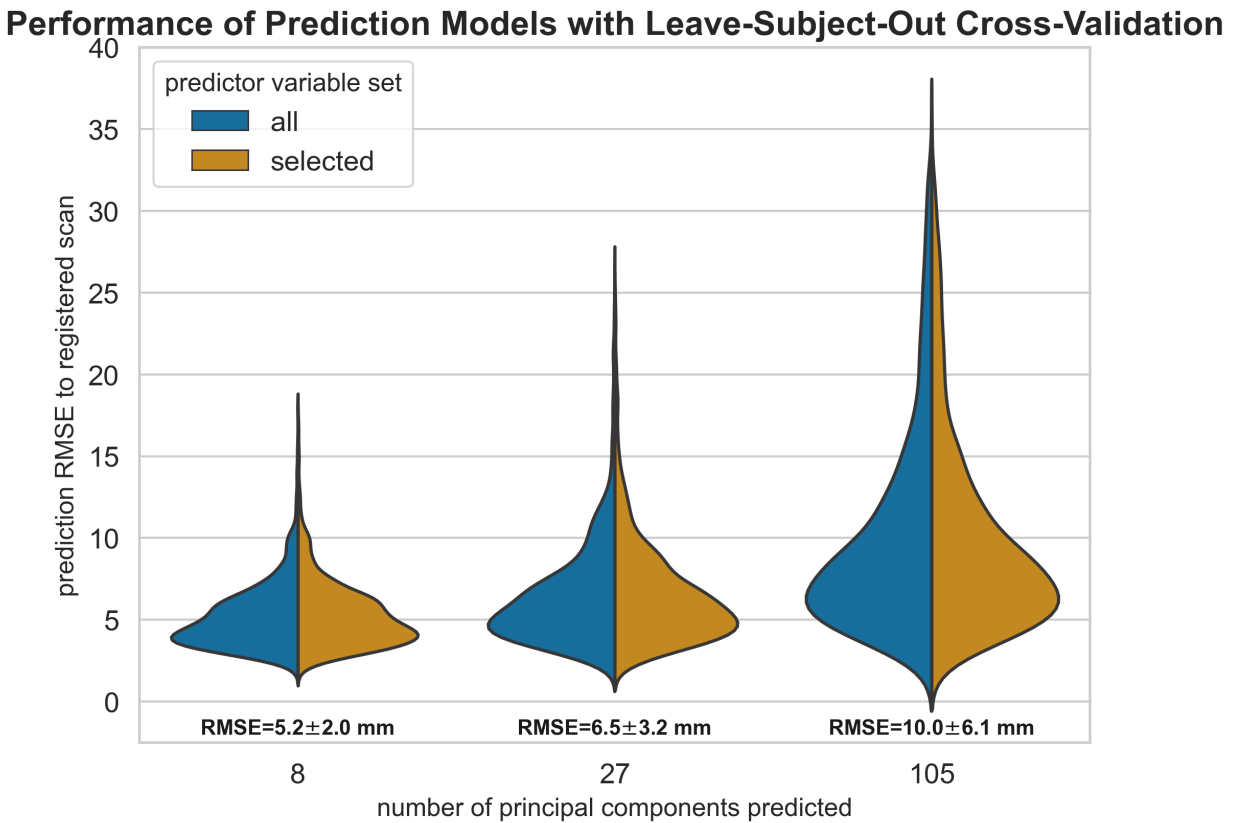


Figure 5.6: Distribution of errors across the various prediction models leave-subject-out cross-validation results. Model RMSE mean and standard deviation are shown above each distribution

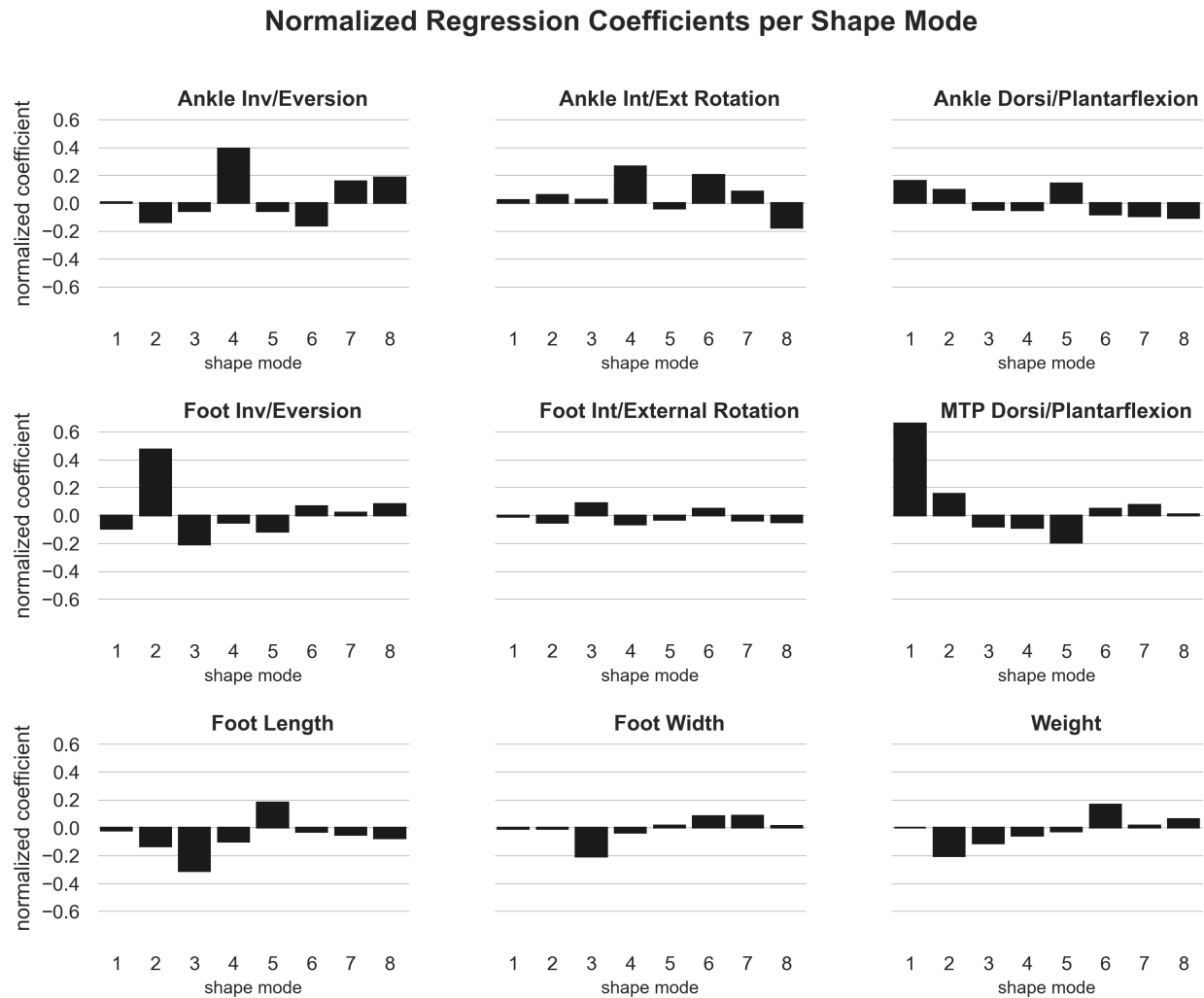


Figure 5.7: Each graph represents the predictor's effects on the shape mode by visualizing the model's normalized coefficients. Larger absolute values indicate a larger effect from the predictor on the shape mode.

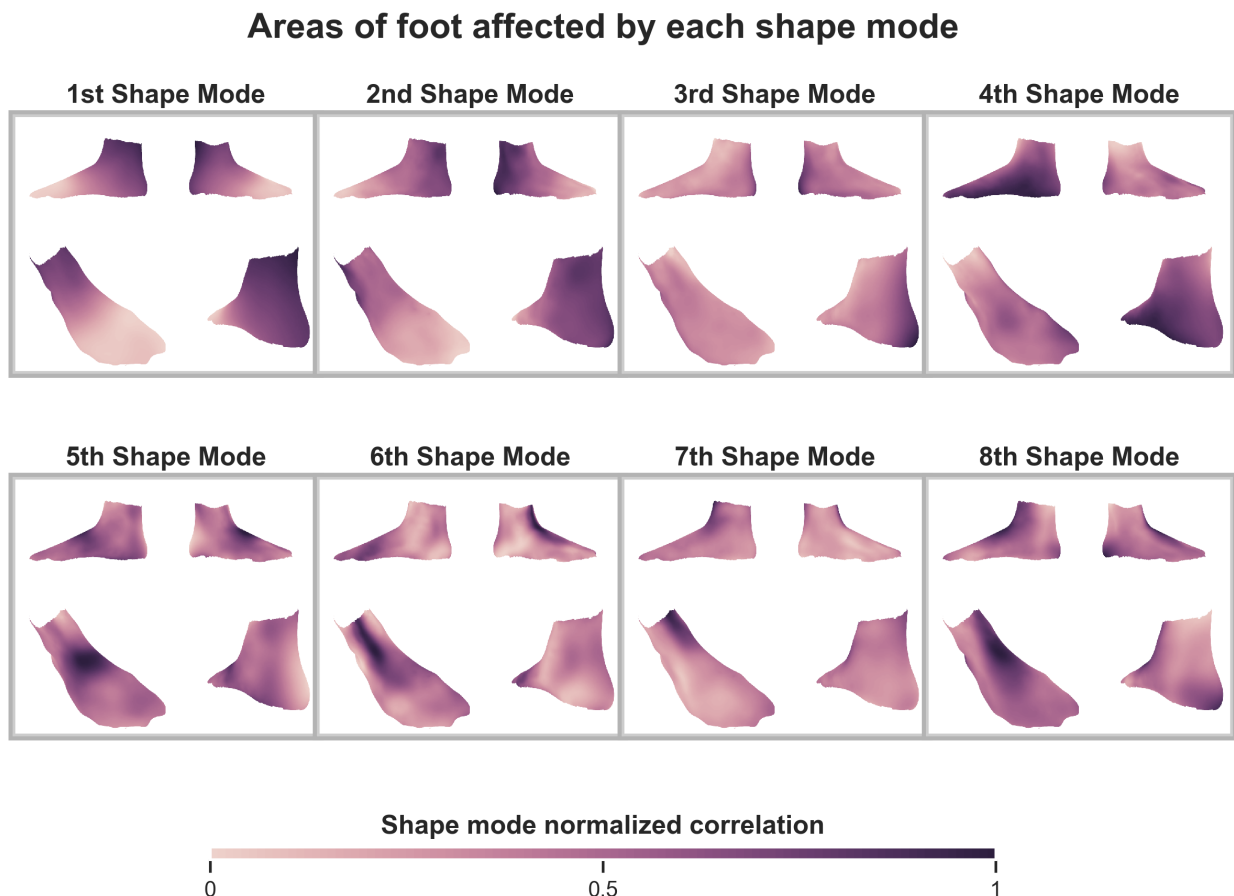


Figure 5.8: Each shape mode's principal axis represented as a heatmap overlaid on the mean foot and shown from 4 different point-of-views. The darker regions represent vertices which are most correlated with the shape mode's principal axis, and therefore see deformations in the shape mode.

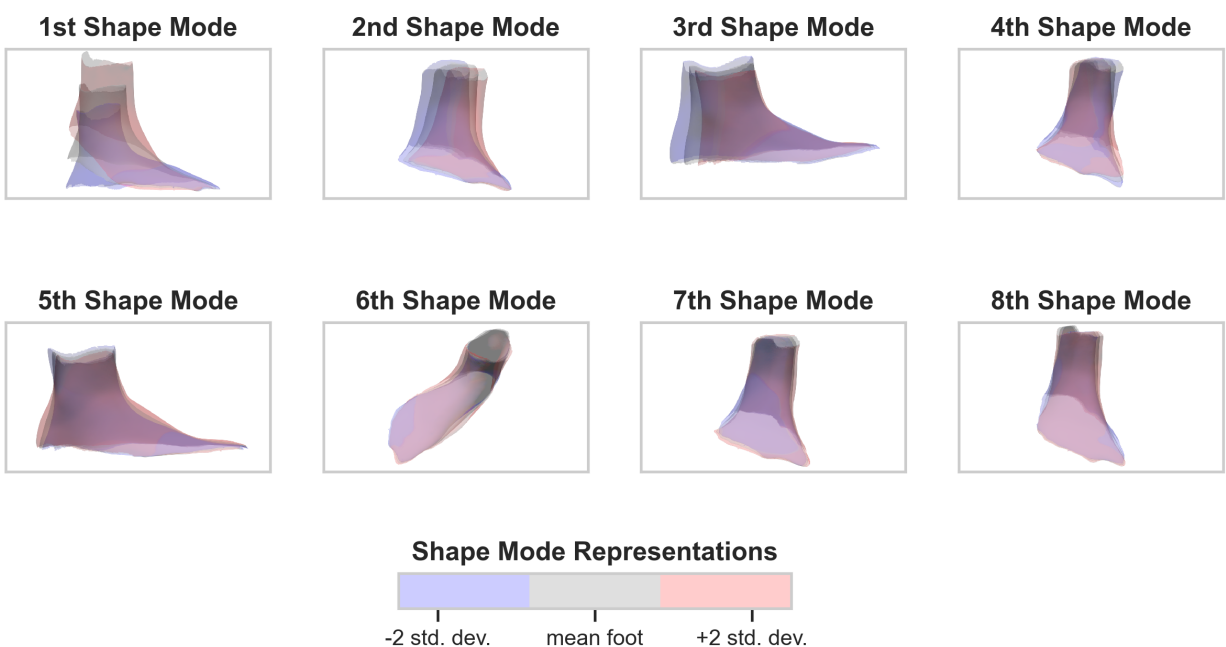
Deformations along each shape mode's axis

Figure 5.9: Foot shape deformation at ± 2 and -2 standard deviations along each shape mode's principal axis, overlaid on the mean foot. The point-of-view is set to highlight the major variance along each shape mode's axis.

foot bones with much lower RMSEs from sparse anatomical landmarks (1.21-1.66 mm for various foot segments) [49] but was trained with higher resolution MRI images. Other efforts to create statistical foot shape models did not incorporate parametric prediction of foot shape [28, 117].

5.3.3 Foot Shape Changes

The first, second, and fourth shape modes, accounting for a total of 86.7% of total variance, capture gross foot motion. Foot motion during stance is dominated by MTP and ankle dorsi/plantarflexion [73], which is captured in the first shape mode (fig. 5.9). The second and fourth shape modes capture gross changes in foot rotation from frontal and transverse plane movements at the MTP and ankle joints, respectively (fig. 5.9). The second shape mode is most affected by foot inversion/everison around the MTP joint. The second shape mode also captures girth scaling at the ankle joint, as seen in (fig. 5.9) by how the ankle girth decreases along the axis, and is affected by weight (fig. 5.7). The fourth shape mode is affected by ankle inversion/eversion and internal/external rotation. Foot inversion/eversion, ankle inversion/eversion, and ankle internal/external rotation are expected to vary across the stance phase ([73]), which leads to the observed changes in gross movement. However, the second and fourth shape modes are slightly affected by foot length, which may suggest inter-individual effects in foot inversion/eversion, ankle inversion/eversion, and internal/external rotation during gait. There is a slight correlation between these angles and foot length (see supplementary figures), which may be due to differences in cadence when walking at the treadmill's set speed. Individuals were given time to acclimate to the treadmill's set speed, but the speed may not have been their preferred walking speed.

The third shape mode captures foot shape scaling at the rearfoot, as highlighted in (fig. 5.8). Foot length shrinks when moving positively along the third shape mode (fig. 5.9), and thus has a negative effect from foot length. There are also negative effects from foot width and weight, which may be due to their correlation to foot length (see supplementary figures). Rearfoot morphology along this shape mode has a more rounded shape in the negative direction, and a sharper shape in the positive direction (fig. 5.9). There is also a negative effect from foot inversion/eversion (fig. 5.7),

indicating that with foot eversion, a sharper rearfoot shape is expected. This may be due to foot eversion at heel-off [73], where the foot unloads from a rounder weight-bearing rearfoot to a sharper non-weight bearing rearfoot shape.

Midfoot girth increases and the rearfoot is rounder along the fifth shape mode's axis (fig. 5.9). The fifth shape mode is positively affected by foot length and negatively by MTP dorsi/plantarflexion (fig. 5.7). This suggests that static midfoot girth increases with foot length, and decreases through heel-off as the MTP dorsiflexes. Rearfoot morphology is rounder for longer foot lengths but gets sharper through heel-off with MTP dorsiflexion, much like in the third shape mode. Midfoot girth was previously found to decrease during stance phase compared to statically standing [50], most likely due to intrinsic and extrinsic foot muscle contraction [113, 44]. However, it was not noted where during stance phase midfoot girth decreases, but it can now be assumed it occurs during heel-off.

The sixth shape mode captures girth changes at the ankle, midfoot, and the medial MTP joint region (fig. 5.8), with girth increasing along the axis. There are positive effects from ankle internal/external rotation and weight, while there is a negative effect from ankle inversion/eversion ([fig:coefs]). Static MTP, midfoot, and ankle girth may therefore increase with subject weight. Dynamic girth changes in these regions may occur as the ankle everts and internally rotates just prior to toe-off, where muscle activation is needed to push the foot off the ground. The foot is stiffened through tension in the MTP joints in order to prepare for toe-off [55], and the MTP joints are known to move relatively within the foot during gait [129, 74] which may be resulting in the increased girth at the MTP joint. A similar mechanism may be occurring at the ankle joint during ankle inversion and internal rotation, where tension from muscle activation prior to toe-off may cause increased girth.

The seventh and eight shape modes, accounting for 1.3% of total variance, capture girth increases near the medial malleolus along their axes (fig. 5.8). They are both positively affected by ankle inversion/eversion (fig. 5.7), and the eighth shape mode is further negatively affected by ankle internal/external rotation. This may suggest that the girth around the medial malleolus decreases

prior to push-off, as the ankle everts and internally rotates.

Observed girth changes at the ankle joint, medial malleolus, midfoot, and MTP joint can be directly mapped to footwear design recommendations for increased fit and comfort. Midfoot girth decreased as the MTP joint is dorsiflexing after heel-off. Midfoot, ankle, and MTP joint girth increased and medial malleolus girth decreased through ankle eversion and external rotation just prior to toe-off. Footwear should be designed to follow these volume changes as the footwear itself goes through the same motions, to ensure proper support for the foot to drive the footwear through the stance phase and toe-off. For example, footwear may be designed to first contract as the MTP joint dorsiflexes, then subsequently expand around the midfoot, ankle and MTP joints while contracting around the medial malleolus as the ankle everts and externally rotates.

5.3.4 Study Limitations

A number of limitations in this study should be noted. The elastic-net method is able to retain cross-correlated predictors, but still requires some bias in the dataset to predict scenarios where cross-correlated predictors are independent [136]. Therefore, the presented model may not be valid for predicting changes in morphology due to independent changes in joint angles outside of stance phase, or for variance in foot width or weight compared to foot length not captured in the subject population.

The model did not capture differences between male and female feet. Studies found that sex differences in foot shape after scaling for foot length were not significant [69, 10, 28], or were small in magnitude [130, 71]. No subject demographic data was collected to account for differences in foot shape due to ethnicity [60]. No data was captured on the foot's plantar surface due to limitations with the scanning system; therefore foot arch changes were not captured. Data captured around the toes had high noise, which necessitated smoothing the toes in the template to ease fitting. Future advances in 4D scanning may alleviate some of these concerns, and also allow for expansion of this model to higher frequency foot motions, such as running.

5.4 Instep Height and Girth Analysis

One of the primary findings in this study was the decrease in midfoot girth through heel-off, but the exact change in measurement was not taken in this study. This region is represented by the traditional foot measurements of instep height and instep girth. Therefore, a in-depth sizing analysis will be conducted in collaboration with Volumental, focusing on these measurements. Jurca et al [60] found that instep height in the median 90% of the population had a range of 16.2 mm, measured from a sample of Volumental's database. The model can be extended by measuring the change in instep height and instep girth with the dynamic foot morphology model. Instep height will be measured across the kinematic variables, foot length, and foot width with the method outlined in Jurca et al [60], to maintain consistency. The range of dynamic instep height will then be compared to the distribution of instep height per length class, done by Jurca et al (2019). From this analysis, it is expected that tolerances for instep height can be defined across the population; specifically, the range needed to capture the median 90% population for each foot length class. Recommendations for how to scale instep height to foot length and foot width can then be generated.

If desired, this analysis can be repeated for the measures of foot length, foot width, and heel width. Correlations between these and additional measures can be explored to find measurements that accurately predict foot shape. This opens the door to generating representative foot shapes for the median 90% of the population; identifying such variables will help prioritize foot measures important to footwear design and fitting.

5.5 Summary

A 4D scanning system was developed to capture dynamic foot shape changes, and was used to collect data for development of the model. To the authors' knowledge, this is the first parametric foot SSM that captures and reconstructs dynamic motion. The model was able to identity specific changes in foot morphology as they related to subject and kinematic parameters, and suggest footwear design techniques to increase fit and comfort. The model is able to reconstruct a full 3D

model when parameter values are provided, which offers a design starting point for constructing a planetary spacesuit boot prototype in Specific Aim 3.

To date, all data-collection for Specific Aim 2 has been completed. A journal paper detailing the development of the 4D scanning system was published in the Journal of Open Source Software. A journal paper detailing the development of the model is currently under review, and has been released as a preprint. The sizing analysis is just starting and will be presented in a future journal paper.

Chapter 6

Specific Aim 3: A design methodology integrating shape modeling into planetary spacesuit boot design

6.1 Introduction

The design for any new spacesuit component should aim to match the required human motions for the intended actions, as well as be sized for the intended population. This allows for the component to provide proper fit and mobility to the wearer, but requires a proper understanding of human size and movement to design. Combining the dynamic foot morphology model with known foot shape and mobility characteristics provides the necessary information to better fit spacesuit components. However, there is not a clear process for integrating all available data to drive spacesuit component design with a focus on improved fit and mobility. This object aims to define that process specifically for the spacesuit boot, through the following objectives:

- Literature review of existing foot shape and mobility knowledge
- Development of a biomechanical framework to design a more compatible spacesuit boot
- Design and construction of a spacesuit boot prototype

6.2 Existing Knowledge on Foot Shape Mobility

Specific foot measures which are directly related to fit and mobility need to be identified to feed into the proposed design framework. Many of these measurements have been characterized through previous analyses^{28–31}. The following sections describe each of these specific foot mea-

sures and provide their population-derived nominal values. fig. 6.1 highlights these foot-specific measures.

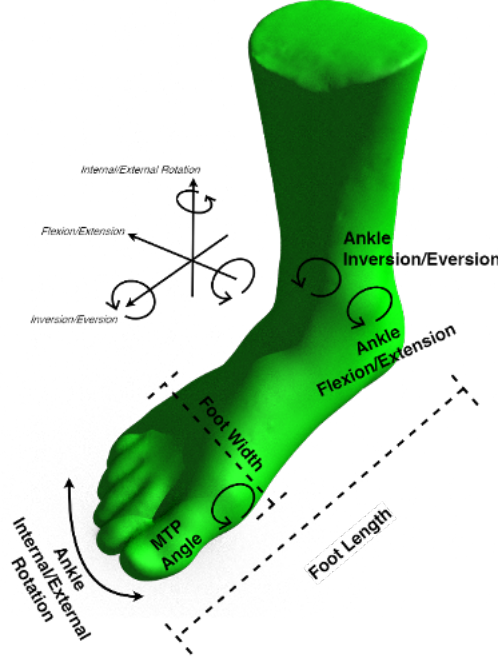


Figure 6.1: Foot-specific measures which directly affect mobility and comfort

6.2.1 Linear Anthropometry

The ANSUR II survey collected a number of foot-related measures which can be analyzed to provide a baseline for foot shapes and sizes[47]. Three of these measures are directly related to fit and mobility. Foot length and foot width define the outer bounds of the foot shape. Foot length and width are directly correlated to US shoe sizes for both width and length. Since females generally feature smaller feet than males, female shoe size is typically 1.5 units less than the calculated male size. Figure 3a shows that this offset does not sufficiently align the female population to the male population. Therefore, it is important to use foot length as a direct measure when fitting or selecting a shoe as opposed to shoe size.

Arch length denotes the location of the metatarsophalangeal (MTP) joints on the foot, one of the important joints during gait. Since power is transmitted through the MTP joints, the

alignment of the MTP joints with the ball of the shoe is important to ensure power is properly transmitted during heel-off. Therefore, the arch length measurement is correlated to standard shoe sizes and if larger, will be selected over the length measurement. Figure 3b shows that while arch length is correlated to foot length for both males and females, there is still high variability in this relationship. Therefore, arch length is an important measure to consider to ensure proper indexing and dynamic fit between the wearer and spacesuit boot.

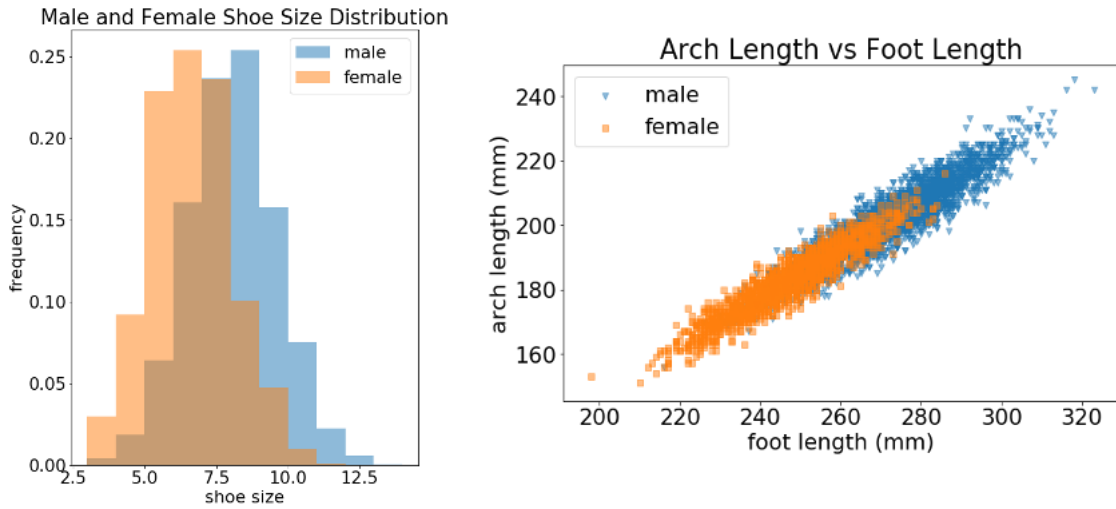


Figure 6.2: (Right) Inequality in distribution of equivalent shoe size between male and female, (Left) relationship between foot length and arch length; visualizations developed from the ANSUR II Dataset

6.2.2 Gait Joint Kinematics

The foot's main function during gait is to transmit power against the ground, ensuring that the human pushes off and initiates a step. During each step, the ankle pushes off from the ground to initiate a step. Intrinsic foot muscles help stiffen the foot to assist the push-off from the ankle against the ground[35]. The MTP joint not only exhibits flexion in the sagittal plane, but provides the necessary stiffness to allow for the ankle power to translate into push off[118]. Ankle joint rotation may also help balance and stability during gait, particularly on slopes[127]. Neither the ankle joint nor the MTP joint should be restricted in its movement to enable efficient push-off and

stability. However, free movement of the ankle joint can increase the risk of injury from instability caused by external forces from walking on an uneven surface. Therefore, there is a balance to be struck between allowing for movement while preventing potentially injurious movements.

Nominal values for the foot MTP and ankle joint movement during gait can be derived from the numerous studies conducted on human gait. [125] found that during gait on uneven surfaces, the ankle does not flex past +/- 20 degrees. [127] reported peak foot-floor angles which suggest that on level and sloped surfaces, subjects dorsiflex their ankle up to 40 degrees, and flex their MTP joint up to 60 degrees. The MTP joint has been shown to flex between 70-90 degrees during gait[79]. There is very little ability of the MTP joint to extend or move in the frontal or transverse plane[79]; these motions therefore do not have to be limited by an MTP joint on the boot.

The ankle joint exhibits most of its movement in the sagittal plane. However, the ankle joint can perform inversion/eversion in the frontal plane and internal/external rotation in the transverse plane. [127] found that subjects wearing a low-top shoe with no additional ankle stability had up to 10 degrees eversion and 15 degrees inversion while navigating a slope. However, excessive inversion/eversion may decrease stability and lead to injury. During gait, the human normally exerts energy to stabilize their ankle in this direction[94]. However, any external force can destabilize the ankle, as commonly seen in basketball or hiking[14]. Therefore, it will be desired that any boot stabilizes the ankle in this motion. In addition, freedom in the transverse plane is desired to allow for positioning of the foot when navigating an uneven surface, aiding in balance[127, 43]. [127] found the ankle internally/externally rotates +15/-20 degrees on a slope.

6.3 Biomechanical Boot Design Framework

The proposed design framework will link foot measurements described in the previous section and the dynamic foot shape model to specific footwear design variables, allowing for the design of a spacesuit boot with proper fit and mobility. The framework assumes the development of a gas-pressurized spacesuit boot to maintain compatibility with the current xEMU architecture. Since gas pressurized spacesuits are stiff when pressurized, they require specially designed joints which

allow for flexibility of the stiff structure. The gas pressurized layer does not have the ability to stretch once pressurized, and therefore must be sized specifically to fit the population range.

Footwear design variables are categorized as either population measures or individual measures. Population design variables are used in the general design and selections of materials for the shoe, which will accommodate the range of foot shapes and motions seen by the population. Individual design variables will be sizing specific elements which are changed between sets of boots to fit inter-individual differences (such as shoe size). fig. 6.3 shows how each foot measurement is mapped to each footwear design variable.

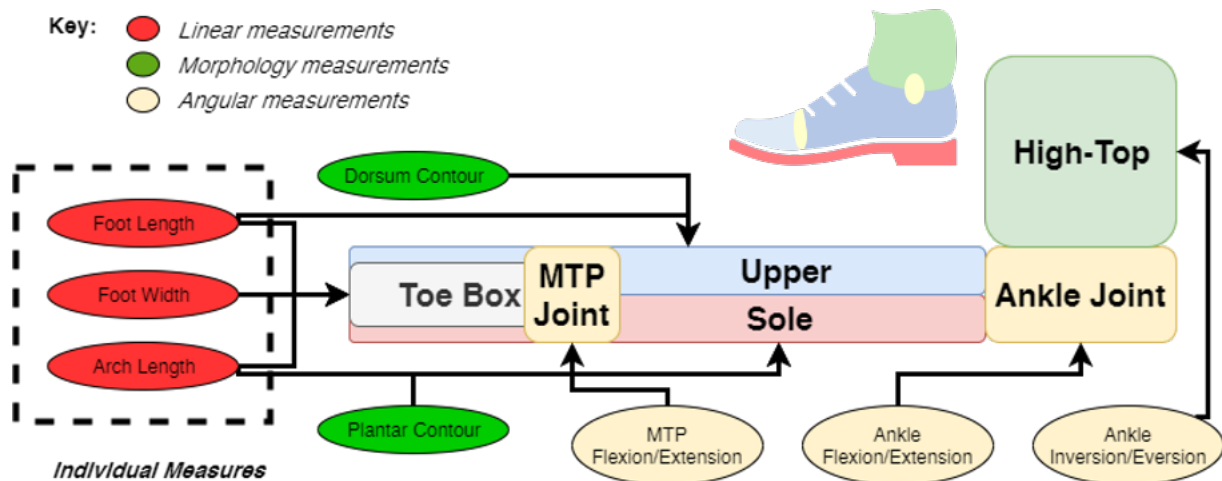


Figure 6.3: Overview and classification of measurements to footwear design variables with representative shoe

6.3.1 Mobility

Footwear is flexible at the MTP and ankle joints to allow for effective push-off during gait. Terrestrial footwear normally derives flexibility from the materials used for that portion of the shoe; the shoe is typically made of softer materials or less reinforcement at the joints. Since altering materials property stiffness is not an option for spacesuit design, rolling convolute or toroidal joints could be used in the spacesuit footwear to allow for flexibility at the MTP and ankle joints[54]. fig. 6.4 shows the desired flexibility based on foot-specific measures. These population measures

will ensure that the boot provides enough flexion to not constrict natural motion.

The MTP joint should target flexion of +90 degrees and the ankle joint should target dorsiflexion/plantarflexion of +40/-20 degrees. Due to the potential for unstable terrain, a high top style footwear is suggested to stabilize the ankle, similar to a hiking or military style boot. However, it has been shown that a very stiff boot reduces ankle ROM and decreases stability at the knee joint [14], potentially leading to ankle and knee fatigue. By allowing for internal/external rotation of +15/-20 degrees, and inversion/eversion of +15/-10 degrees, the boot still allows the foot to navigate a sloped and uneven surface without fatigue. The relatively low amount of movement will still allow the ankle to be stabilized and lower the risk of injury.

The only requirements previously stated for boot mobility are in the 2019 NASA SBIR Surface Space Suit Boot Solicitation [88]. The solicitation matches the +40/-20 degrees ankle dorsiflexion/plantarflexion requirement, but presents no requirements for ankle internal/external rotation, inversion/eversion, or MTP joint flexion. The proposed design framework targets higher flexion/extension capability in the ankle joint, as well as specifies extension of the MTP joint, limited ankle internal/external rotation, and limited ankle inversion/eversion.

6.3.2 Toe box

The toe box accommodates the foot forward of the MTP joint. The toes provide the contact for power from the MTP and ankle joints to push off the ground during each step. Therefore, the most important feature of the toe box is contact between the toes and the ground during heel-off. As a result, the toe box can feature more space around the top of the toes for comfort [76]. Since the toe box does not need to provide any additional flexibility, it can be constructed with a less flexible, harder, material to allow for adequate support of the boot and foot. In conjunction with the MTP joint, the toe box should also be adjustable such that it can match the arch length of the wearer, allowing for proper fit and indexing of the MTP joint.

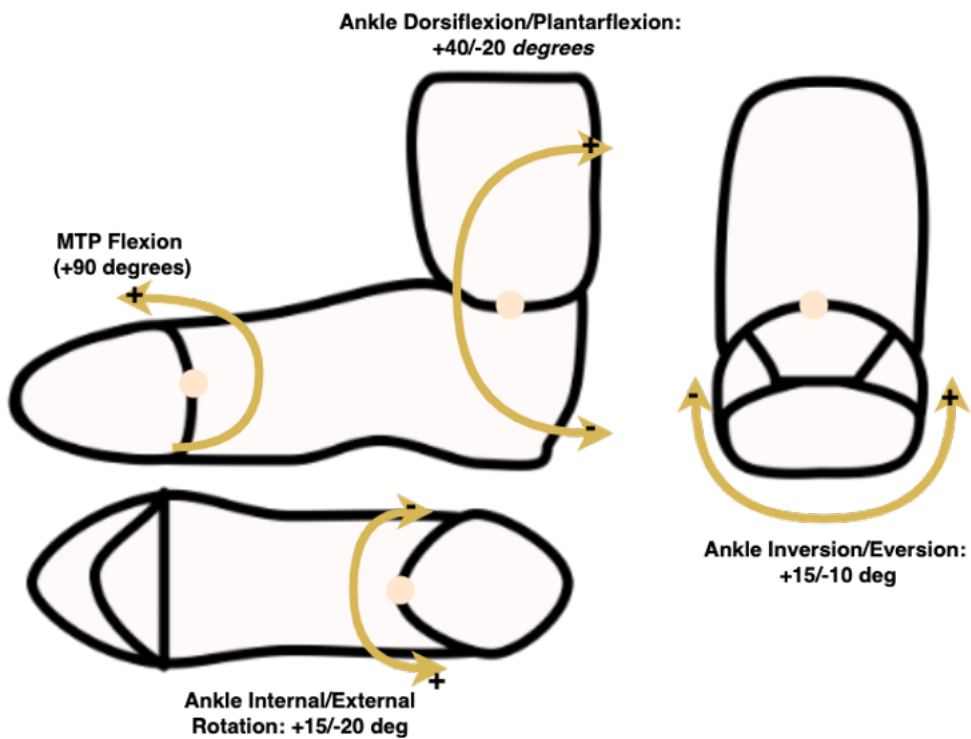


Figure 6.4: Mobility and flexibility of joints needed in the spacesuit boot

6.3.3 Upper

The dorsum of the foot is covered by a shoe upper. The shape of the upper needs to conform to the shape of the dorsum to allow for proper driving of the shoe during any activity [36]. Foot shape data taken from a large population will be useful in defining an ideal upper shape that fits a range of persons. The boot upper will also have to conform to the foot shape without causing discomfort during movement. Dynamic foot shape data can quantify how dorsum shape is changing throughout the gait cycle, allowing for the upper to accommodate any expansion or contraction of the dorsum shape for optimal comfort and support. The dynamic foot shape model drive the design of an upper which can be easily scaled to different shoe sizes.

The upper's location between the MTP and ankle joint, and its requirement to conform to the shape of the foot, drive the selection of a softer, flexible fabric being used to meet these requirements. This presents a challenge with designing the pressure bladder, as the pressure bladder is inherently stiff under pressure. Therefore, a soft inner layer above the dorsum may be used which allows the stiff pressurized bladder to conform to the individual's dorsum. Since the dorsum still transmits power to push the shoe off the ground, the soft layer still needs to have enough structure to transmit this power. If too soft, the layer will simply act as empty space and the shoe will not respond to ankle flexion during heel-off, potentially resulting in heel-lift. Lacing or other closure mechanisms would further allow the shoe upper to conform to the dorsum and capture the foot. Furthermore, the closure mechanism should be customizable by the individual wearing the boot, so each wearer can adjust to where they feel is comfortable. Conforming the upper to the dorsum will also minimize contact injuries between the wearer and boot.

The upper will also play a role in donning and doffing of the spacesuit boot. Traditional boots feature laces along the upper which secure the foot inside the boot during activity, but loosen to allow the foot to slip into and out of the boot. The closure can be designed in conjunction with a single structured fold in the pressure bladder to allow the pressure bladder to change shape and allow the foot to be released from the boot. fig. 6.5 shows a possible configuration of the upper

using laces which conforms to the shape of the foot while still allowing for donning and doffing.

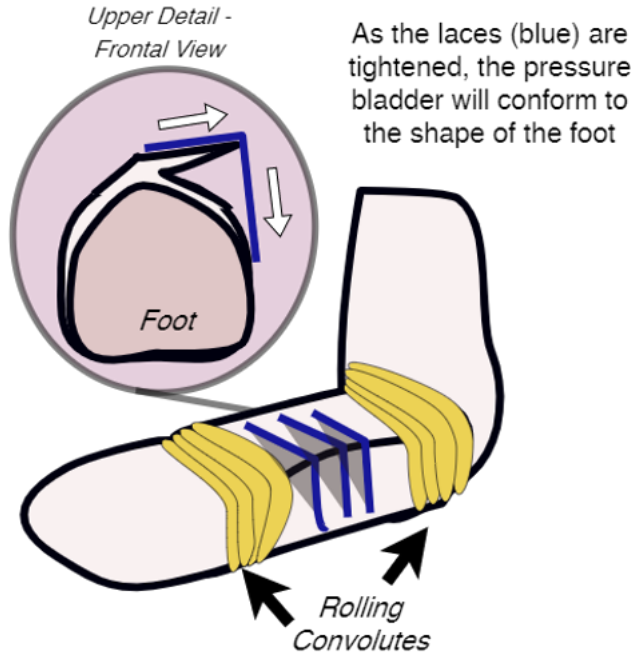


Figure 6.5: Conceptual design of a boot's upper configuration with pressure bladder

6.3.4 Sole

The sole in a traditional boot provides traction, support, and protection to the wearer. The sole needs some thickness to accommodate tread for grip on uneven surfaces. In general, the thicker a sole, the stiffer it becomes. As a stiff sole resists bending, it might fight against the motion of the foot and shoe during heel-off. Therefore, the sole needs to be flexible during heel-off without imparting additional forces on the shoe and upper. Dobson et al (2020) found that having a fully flexible sole in coal miner's boots inhibited the natural roll-off of the foot during gait, resulting in less comfort [32]. However, it was not verified if the boot's flexibility at the MTP joint aligned well with the MTP joint, since sole flexibility was done simply by cutting into the sole near the MTP joints. Therefore, it will be imperative to ensure that any flexibility at the MTP joint is either perfectly aligned with the foot, or the flexibility does not inhibit the natural roll off of the foot.

Dynamic foot shape data can provide a base contour for the sole to be able to bend at the MTP joint during heel-off, as shown in fig. 6.6. The sole should have higher flexibility near the MTP joints; doing so will allow the sole curvature to match the foot's plantar curvature during gait. In addition, population measures of arch length can help characterize the location of the MTP joint along the foot, ensuring that the MTP joint is properly indexed by the sole.

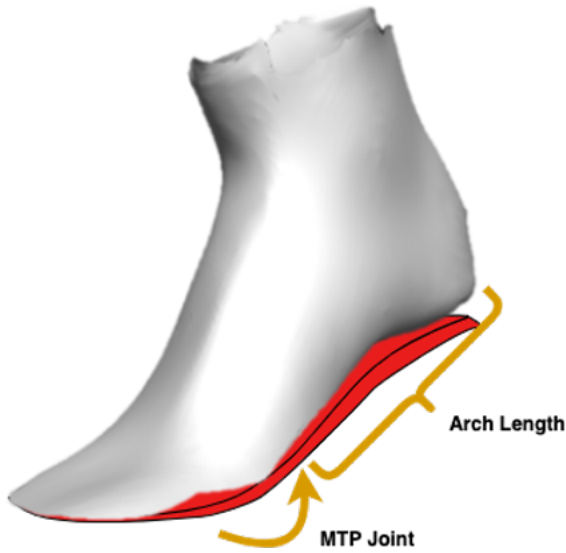


Figure 6.6: Desired sole flexibility (red) matched with plantar foot contour at MTP joint

6.4 Prototyping Construction Plan

6.4.1 Design Process

The resulting boot design from this framework and corresponding computational analysis will serve as a starting point for iteration of a spacesuit boot prototype. Due to the difficulty of developing a pressurized boot, an existing boot will first be made pressurized as practice. Heat-sealable urethane coated nylon (400D, Seattle Fabrics) will be used for the pressure bladder, which was recommended by spacesuit professionals. It is expected that a target pressure between 3-5 psi

will be reached with this design; for reference, the operating pressure of the EMU spacesuit is 4.3 psi.

A collaboration between CU and the University of Oregon Portland will first create a baseline design around the presented requirements. The pressure bladder will be fixed to the inside of the shoe using a series of tabs, ensuring that it is always indexed properly inside the foot. The rolling convolute and toroidal joints will be designed with well-established methods [54]. The upper layer will require a specifically designed restraint layer to capture the dynamic motion of the midfoot during gait. A collaboration between CU and BOA Technologies will incorporate the use of BOA laces into the restraint layer to capture the midfoot. For ease of construction, prototypes will be constructed to one selected test subject's shoe size. For comparison in Specific Aim 4, a MK III-esque hiking boot will also be constructed with only a constant-volume ankle joint.

6.5 Summary

This analysis outlined a framework for designing a new spacesuit boot with an emphasis on fit and mobility during gait. The framework aims to reduce the risk of spacesuit boot injury by developing a process to design a spacesuit boot. It is expected that focusing a design on fit and mobility will reduce the occurrence of heel-slip and contact injuries.

This framework therefore serves as bounding requirements to ensure future spacesuit footwear does not inhibit natural foot motion or cause discomfort due to incompatibilities between foot and shoe shape. The only previously bounding requirement, the 2019 NASA SBIR solicitation for a new surface space suit boot, had only one requirement for ankle flexion/extension, which was validated in this paper. There were no requirements other ankle motions or MTP joint motions, and no requirement for proper static and dynamic fit to the wearer's foot. This work provides a series of requirements based from previous biomechanics studies on foot motion while walking and hiking to provide proper fit and mobility through the spacesuit boot design. Prototypes constructed from this work will be validated in Specific Aim 4.

As of Fall 2020, the literature review and biomechanical design framework have been com-

pleted. Work is currently starting on the prototype spacesuit boot design and construction. The literature review and biomechanical design framework have been presented in a paper published at the 2020 International Conference on Environmental Systems Meeting. The final design of the boot will be presented in a future journal paper and conference presentations.

Chapter 7

Specific Aim 4: Evaluation of prototype planetary spacesuit boot design for fit and comfort

7.1 Introduction

The pressurized boot prototype developed in Specific Aim 3 will need to be validated to test the main of this thesis. The gold-standard of EVA mobility would be an unpressurized hiking boot. Current MK III boots feature only a convoluted ankle joint [107]. The prototype will be compared against these two boot options, essentially testing the effects of boot pressurization with ankle mobility and the midfoot indexing feature designed in Specific Aim 3. The prototype will be mated to a glovebox to allow for pressurized testing. If achievable, the prototype will also be tested in walking trails outside of the glovebox. Since the boots will be constructed to only fit one subject, therefore, testing with multiple subjects will be difficult unless subjects with similar foot shape are found. Regardless of test-setup, the main objectives of this work are:

- Construct interface between test boots and test environments
- Evaluate the mobility of the novel design against a standard hiking boot and pressurized hiking boot
- Evaluate the comfort of the novel design against a standard hiking boot and pressurized hiking boot

7.2 Test Interface Construction

Interfaces will need to be constructed between the boots to be tested and the test environments. For the glovebox testing, the interface will need to allow for pressurization of the prototype boot and the MK III boot. When a vacuum is pulled inside the glovebox, the boot will become pressurized with the ambient air. The standard hiking boot will also need an interface to the glovebox to offer similar testing conditions, but will not need to be pressurized.

Another potential interface will be mate the pressurized boots to the shank of the wearer. This interface will require some sort of seal around the wearer's ankle. Due to expected imperfections in the seal, the boot will most likely be fed with constant pressurized air to maintain a constant pressure. This interface will first be tested on the practice boot constructed in SA3 before being incorporated into the prototype and MK III boot.

7.3 Glovebox Testing

All three boots will be mated to the glovebox, and a vacuum will be pulled to the limits of the boot design and glovebox. A force sensor will be placed in the heel of the boot, in as minimally intrusive position as possible. This sensor will be used to measure for the presence of heel-lift. If possible, a sensor which can measure distance between the sole and heel will be selected for this application.

The glovebox will be placed on the ground, with the subject in a standing posture. The subject will perform range-of-motion tests of their ankle inside the glovebox. Motions will be performed both unloaded, where the boot is free in the air, and loaded, where the boot is pushing against a flat floor. This is consistent with previous planetary boot testing methodology [107]. The subject will also perform a series of heel lifts to test for heel-lift. Range-of-motion will be measured with photogrammetry, taken from the front and side profile, and used to assess mobility

Subjective surveys will be provided to the subject to fill after finishing the range-of-motion tests. The Corlett-Bishop Discomfort Scale [29], Rating of Perceived Exertion Survey [16], and

Gravity compensation and performance scale (GCPS) [45, 92, 91] will be used to assess subjective comfort of the boots.

7.4 Stretch Testing Goals

The glovebox testing will provide initial insight into comfort and mobility, but will be limited in translation as it does not include walking. If a pressurized seal around the ankle is achievable, a biomechanical walking evaluation of the three boots can occur. Walking will occur on a flat walkway, where the subject will walk across force plates to measure ground reaction forces. Optical motion capture will be used to capture segment kinematics of the lower torso. A kinetic analysis from the kinematics and ground reaction forces can provide information on joint torques at the ankle, knee, and pelvis. The aforementioned subjective surveys will be administered following data collection with each boot. If spacesuit testing is available through collaborators at David Clark or NASA JSC, the prototype will be integrated into the spacesuit and similar measures will be taken.

7.5 Summary

This work will evaluate the fit and mobility of the boot designed in Specific Aim 3. Results from this work will directly inform the performance of a boot designed with body-shape modeling techniques. This work will not be started until Specific Aim 3 is complete, as it depends on the delivery of the prototype boot.

Chapter 8

Execution Plan

Through many advancements of planetary EVA spacesuit design, operator-spacesuit coordination is still not perfectly matched. Poor mobility and poor fit between the operator and spacesuit are some of the most common factors that can lead to injury. The boot subsystem of the MK III has shown to not be properly fit or match the mobility of the ankle, creating a phenomenon known as heel-lift. This research showed the capability of heel-off detection differences between the operator and spacesuit to indicate presence of heel-lift during gait. The dynamic foot shape model developed in this work can predict and provides insight into how the foot moves and changes during stance phase. A design framework was proposed to design a planetary EVA spacesuit boot that incorporates existing knowledge on foot mobility with the dynamic foot shape model. A prototype spacesuit boot will be designed around this framework, and be tested for comfort and mobility against a standard Earth hiking boot and a MK III-inspired pressurized boot. Results from this testing will validate the use of dynamic body shape models in spacesuit component design, while the framework and model will provide a path to create the models and design spacesuit components from them.

8.1 Timeline

The Gantt chart below shows the timeline for each specific aim of the thesis and for PhD graduation milestones.

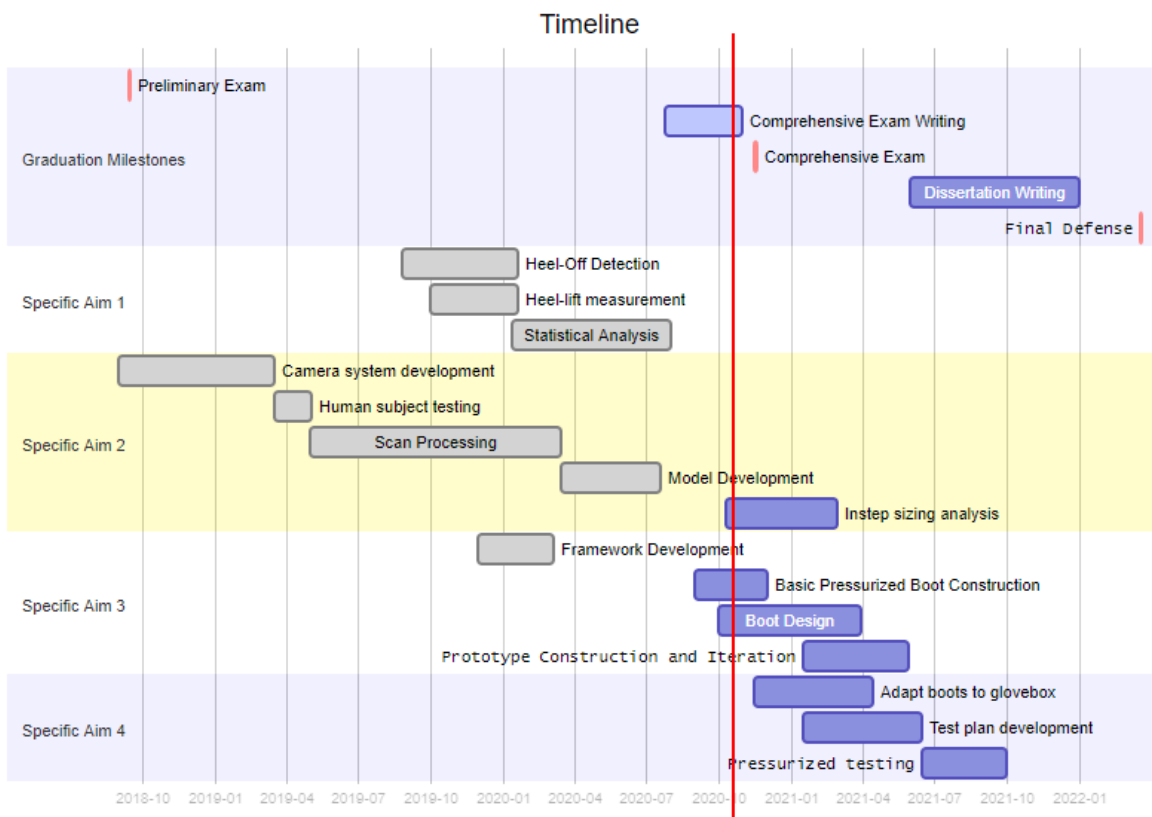


Figure 8.1: Gantt chart showing PhD timeline

8.2 Publication Plan

tbl. 8.1 outlines the peer-reviewed conference and journal papers from this thesis work. tbl. 8.2 outlines conference presentations and posters from this thesis work. Publications and presentations which are proposed and subject to having their title changed.

Table 8.1: Peer-reviewed publications

Type	Title	Journal	Status
Technical Note	Detecting Heel-Lift in Spacesuit Gait	Aerospace Medicine and Human Performance	In Preperation
Journal Paper	DynaMo: Dynamic Body Shape and Motion Capture with Intel RealSense Cameras	Journal of Open Source Software	Published
Journal Paper	Dynamic foot morphology explained through 4D scanning and shape modeling	Journal of Biomechanics	Under Review
Conference Paper	A Biomechanical Design Framework to Improve Spacesuit Boot Fit	50th International Conference on Environmental Systems	Published

Type	Title	Journal	Status
Journal Paper	Static and Dynamic Distribution of Instep Height	Footwear Science	Proposed
Journal Paper	Design of A Novel Planetary Spacesuit Boot Design	Acta Astronautica	Proposed
Journal Paper	Comfort and Mobility Evaluation of a Novel Planetary Spacesuit Boot Design	Aerospace Medicine and Human Performance	Proposed

Table 8.2: Conference Presentations and Posters

Type	Title	Conference	Date
Talk	Using dynamic foot morphology data to design spacesuit footwear	Footwear Biomechanics Symposium	July 2019
Talk	Development of a Dynamic 3D Scanning System with Multiple Intel RealSense Depth Cameras	International Society of Biomechanics Congress	Aug 2019

Type	Title	Conference	Date
Poster	Quantifying the Heel Lift during Spacesuit Gait	NASA HRP IWS	Jan 2020
TBD	Dynamic Body-Shape Models to Reduce Risk OF EVA Spacesuit Injury	NASA HRP IWS	Feb 2021
TBD	Novel Spacesuit Boot Design Developed from Dynamic Foot Shape Modeling	Footwear Biomechanics Symposium	July 2021
TBD	Spacesuit Boot with Improved Comfort and Mobility Developed from Dynamic Shape Modeling	NASA HRP IWS	Jan 2022

8.3 Academic Requirements

All required coursework was completed as of the Spring 2020 semester. Of the 36 required credits, 30 were taken in ASEN, with 12 at the 6000 level. MCEN 5228 (Modeling Human Movement) and APPM 5590 (Statistical Modeling) were taken outside of ASEN. The 6 required math credits were exceeded with taking ASEN 5519 (Experimental Design and Statistical Analysis), APPM 5590 (Statistical Modeling), and ASEN 5044 (Statistical Estimation for Dynamical Sys-

tems). As of the Fall 2020 semester, 15 out of the 30 required Doctoral dissertation credits have been taken. The remaining 15 credits will be evenly taken during the Spring 2021, Fall 2021, and Spring 2022 semesters. The teaching practicum has been fulfilled through the mentoring of UROP students in the Summer 2018, Fall 2019, and Spring 2020 semesters. A TA position is also expected in Fall 2021.

natbib

Bibliography

- [1] Isaak P. Abramov, Anatoly Yu Stoklitsky, Arnold S. Barer, and Sergei N. Filipenkov. Essential aspects of space suit operating pressure trade-off. In SAE Technical Papers. Society of Automotive Engineers, 1994.
- [2] Marko Ackermann and Antonie J. Van den Bogert. Predictive simulation of gait at low gravity reveals skipping as the preferred locomotion strategy. Journal of Biomechanics, 45(7):1293–1298, 2012.
- [3] Brett Allen, Brian Curless, and Zoran Popović. The space of human body shapes: Reconstruction and parameterization from range scans. ACM Transactions on Graphics, 22(3):587–594, 2003.
- [4] Ryan Z. Amick, Christopher R. Reid, Scott A. England, and Sudhakar L. Rajulu. Characterization of joint resistance and performance degradation of the Extravehicular Mobility Unit Spacesuit: A pilot study. In Proceedings of the Human Factors and Ergonomics Society 59th Annual Meeting, pages 1259–1263, sep 2015.
- [5] Allison Anderson. Understanding Human-Space Suit Interaction to Prevent Injury During Extravehicular Activities. Phd, Massachusetts Institute of Technology, 2014.
- [6] Dragomir Anguelov, Praveen Srinivasan, Daphne Koller, Sebastian Thrun, Jim Rodgers, and James Davis. SCAPE: Shape Completion and Animation of People. ACM Transactions on Graphics, 24(3):408–416, 2005.
- [7] Erik K. Antonsson and Robert W. Mann. The frequency content of gait. Journal of Biomechanics, 18(1):39–47, jan 1985.
- [8] ASTM F539-01. Standard Practice for Fitting Athletic Footwear. Technical report, ASTM, West Conshohocken, PA, 2017.
- [9] Bettina Barisch-Fritz, Timo Schmeltzpfenning, Clemens Plank, and Stefan Grau. Foot deformation during walking: Differences between static and dynamic 3D foot morphology in developing feet. Ergonomics, 57(6):921–933, jun 2014.
- [10] Bettina Barisch-Fritz, Timo Schmeltzpfenning, Clemens Plank, Tobias Hein, and Stefan Grau. The effects of gender, age, and body mass on dynamic foot shape and foot deformation in children and adolescents. Footwear Science, 6(1):27–39, jan 2014.

- [11] Elizabeth Benson and Sudhakar Rajulu. Complexity of sizing for space suit applications. *Lecture Notes in Computer Science (including subseries Lecture Notes in Artificial Intelligence and Lecture Notes in Bioinformatics)*, 5620 LNCS(June):599–607, 2009.
- [12] Fausto Bernardini, Joshua Mittleman, Holly Rushmeier, Claudio Silva, and Gabriel Taubin. The Ball-Pivoting Algorithm for Surface Reconstruction. *IEEE Transactions on Visualization and Computer Graphics*, 5(4):349–359, 1999.
- [13] Pierre J. Bertrand. Enhancing Astronaut Mobility Spacesuit Kinematics and Interactive Space Outreach. pages 1–225, 2016.
- [14] Harald Böhm and Matthias Hösl. Effect of boot shaft stiffness on stability joint energy and muscular co-contraction during walking on uneven surface. *Journal of Biomechanics*, 43(13):2467–2472, sep 2010.
- [15] Abhishektha Boppana and Allison P Anderson. DynaMo: Dynamic Body Shape and Motion Capture with Intel RealSense Cameras. *The Journal of Open Source Software*, 4(41), 2019.
- [16] G. A.V. Borg. Psychophysical bases of perceived exertion. *Medicine and Science in Sports and Exercise*, 14(5):377–381, 1982.
- [17] G. Bradski. The OpenCV Library. *Dr. Dobb's Journal of Software Tools*, 2000.
- [18] Raymond C. Browning, Emily A. Baker, Jessica A. Herron, and Rodger Kram. Effects of obesity and sex on the energetic cost and preferred speed of walking. *Journal of Applied Physiology*, 100(2):390–398, feb 2006.
- [19] Seonjeong Byun, Hyang Jun Lee, Ji Won Han, Jun Sung Kim, Euna Choi, and Ki Woong Kim. Walking-speed estimation using a single inertial measurement unit for the older adults. *PLoS ONE*, 14(12):1–16, 2019.
- [20] J. Martin Carlson. Functional limitations from pain caused by repetitive loading on the skin: A review and discussion for practitioners, with new data for limiting friction loads. *Journal of Prosthetics and Orthotics*, 18(4):93–103, 2006.
- [21] Christopher E. Carr and Jeremy McGee. The apollo number: Space suits, self-support, and the walk-run transition. *PLoS ONE*, 4(8):1–7, 2009.
- [22] G. A. Cavagna, N. C. Heglund, and C. R. Taylor. Mechanical work in terrestrial locomotion: two basic mechanisms for minimizing energy expenditure. *American Journal of Physiology - Regulatory Integrative and Comparative Physiology*, 2(3), 1977.
- [23] G. A. Cavagna, H. Thys, and A. Zamboni. The sources of external work in level walking and running. *The Journal of Physiology*, 262(3):639–657, 1976.
- [24] Steven P. Chappell. *Analysis of Planetary Exploration Spacesuit Systems and Evaluation of a Modified Par Phd*, University of Colorado Boulder, 2006.
- [25] Steven P. Chappell, Jason R. Norcross, Andrew F.J. Abercromby, Omar S. Bekdash, Elizabeth A. Benson, and Sarah L. Jarvis. Evidence Report : Risk of Injury and Compromised Performance Due to EVA Operations. Technical report, Houston, TX, 2017.

- [26] Chacqueline M. Charvat, Jason Norcross, Christopher R. Reid, and Shane M. McFarland. Spacesuit Glove-Induced Hand Trauma and Analysis of Potentially Related Risk Variables. In *45th International Conference on Environmental Systems*, number July, Bellevue, WA, 2015.
- [27] Yan Chen and Gerard Medioni. Object modelling by registration of multiple range images. *Image and Vision Computing*, 10(3):2724–2729, 1992.
- [28] Bryan P. Conrad, Michael Amos, Irene Sintini, Brian Robert Polasek, and Peter Laz. Statistical shape modelling describes anatomic variation in the foot. *Footwear Science*, 11(sup1):S203–S205, jun 2019.
- [29] E. N. Corlett and R. P. Bishop. A technique for assessing postural discomfort. *Ergonomics*, 19(2):175–182, 1976.
- [30] Conor R. Cullinane, Richard A. Rhodes, and Leia A. Stirling. Mobility and agility during locomotion in the mark III space suit. *Aerospace Medicine and Human Performance*, 88(6):589–596, jun 2017.
- [31] Jessica A. Dobson, Diane L. Riddiford-Harland, Alison F. Bell, and Julie R. Steele. The three-dimensional shapes of underground coal miners' feet do not match the internal dimensions of their work boots. *Ergonomics*, 61(4):588–602, 2018.
- [32] Jessica A. Dobson, Diane L. Riddiford-Harland, Alison F. Bell, Caleb Wegener, and Julie R. Steele. Effect of shaft stiffness and sole flexibility on perceived comfort and the plantar pressures generated when walking on a simulated underground coal mining surface. *Applied Ergonomics*, 84:103024, apr 2020.
- [33] J. M. Donelan and R. Kram. Exploring dynamic similarity in human running using simulated reduced gravity. *Journal of Experimental Biology*, 203(16):2405–2415, 2000.
- [34] Bret G. Drake and Kevin D. Watts. Human exploration of mars, design reference architecture 5.0. Technical report, NASA Johnson Space Center, Houston, TX, 2010.
- [35] Dominic James Farris, Luke A. Kelly, Andrew G. Cresswell, and Glen A. Lichtwark. The functional importance of human foot muscles for bipedal locomotion. *Proceedings of the National Academy of Sciences*, 116(5):1645–1650, jan 2019.
- [36] Daniel Feeney, Brett Vladika, Jay Dicharry, and Bradley Davidson. Upper configurations can affect endurance, agility, and power performance. *Footwear Science*, 11(sup1):S96, jun 2019.
- [37] Raúl Feliz, Eduardo Zalama, and Jaime Gómez García-Bermejo. Pedestrian tracking using inertial sensors. *Journal of Physical Agents*, 3(1):35–42, 2009.
- [38] Richard A. Fineman, Andrew F J Abercromby, Amy Ross, and Leia A. Stirling. Cognitive Task Analysis of Mark III Fit Checks for the Development of Human-Spacesuit Performance Metrics. In *Proceedings of the 47th International Conference on Environmental Systems*, Charleston, SC, 2017.
- [39] Richard A. Fineman, Timothy M. McGrath, Damian G. Kelty-Stephen, Andrew F. Andrew, and Leia A. Stirling. Objective metrics quantifying fit and performance in spacesuit assemblies. *Aerospace Medicine and Human Performance*, 89(11):985–995, nov 2018.

- [40] Richard A. Fineman and Leia A. Stirling. Quantification and visualization of coordination during non-cyclic upper extremity motion. *Journal of Biomechanics*, 63:82–91, 2017.
- [41] Carl Fischer, Poorna Talkad Sukumar, and Mike Hazas. Tutorial: Implementing a pedestrian tracker using inertial sensors. *IEEE Pervasive Computing*, 12(2):17–27, apr 2013.
- [42] Martin A. Fischler and Robert C. Bolles. Random sample consensus: A Paradigm for Model Fitting with Applications to Image Analysis and Automated Cartography. *Communications of the ACM*, 24(6):381–395, 1981.
- [43] John J Fraser, Mark A Feger, and Jay Hertel. Midfoot and Forefoot Involvement in Lateral Ankle Sprains and Chronic Ankle Instability. Part 1: Anatomy and Biomechanics. *The International Journal of Sports Physical Therapy*, 11(6):992–1005, dec 2016.
- [44] A. Gefen, M. Megido-Ravid, Y. Itzchak, and M. Arcan. Biomechanical analysis of the three-dimensional foot structure during gait: A basic tool for clinical applications. *Journal of Biomechanical Engineering*, 122(6):630–639, 2000.
- [45] Michael L Gernhardt, Jeffrey A Jones, Richard A Scheuring, Andrew F Abercromby, Jennifer A Tuxhorn, and Jason R Norcross. Risk of Compromised EVA Performance and Crew Health Due to Inadequate EVA Suit Systems. Technical report, 2009.
- [46] Eugene Giles and Paul H. Vallandigham. Height Estimation from Foot and Shoeprint Length. *Journal of Forensic Sciences*, 36(4):13129J, 1991.
- [47] Claire C. Gordon, Cynthia L. Blackwell, Bruce Bradtmiller, Joseph L. Parham, Patricia Barrientos, Stephen P. Paquette, Brian D. Corner, Jeremy M. Carson, Joseph C. Venezia, Belva M. Rockwell, Michael Mucher, and Shirley Kristensen. 2012 Anthropometric Survey of U.S. Army Personnel: Methods and Summary Statistics. Technical report, ARMY NATICK SOLDIER RESEARCH DEVELOPMENT AND ENGINEERING CENTER MA, Natick, MA, dec 2014.
- [48] Alena Grabowski, Claire T. Farley, and Rodger Kram. Independent metabolic costs of supporting body weight and accelerating body mass during walking. *Journal of Applied Physiology*, 98(2):579–583, 2005.
- [49] Tamara M. Grant, Laura E. Diamond, Claudio Pizzolato, Bryce A. Killen, Daniel Devaparakash, Luke Kelly, Jayishni N. Maharaj, and David J. Saxby. Development and validation of statistical shape models of the primary functional bone segments of the foot. *PeerJ*, 2020(2):e8397, feb 2020.
- [50] Stefan Grau and Bettina Barisch-Fritz. Improvement of safety shoe fit - evaluation of dynamic foot structure. *Footwear Science*, 10(3):179–187, sep 2018.
- [51] Dave Graziosi, Bobby Jones, Jinny Ferl, Steve Scarborough, Linda Hewes, Amy Ross, and Richard Rhodes. Z-2 Architecture Description and Requirements Verification Results Abstract. In *46th International Conference on Environmental Systems*, Vienna, jul 2016.
- [52] Timothy M. Griffin, Neil A. Tolani, and Rodger Kram. Walking in simulated reduced gravity: Mechanical energy fluctuations and exchange. *Journal of Applied Physiology*, 86(1):383–390, 1999.

- [53] Yi Chiew Han, Kiing Ing Wong, and Iain Murray. Gait Phase Detection for Normal and Abnormal Gaits Using IMU. *IEEE Sensors Journal*, 19(9):3439–3448, 2019.
- [54] Gary L. Harris. *The origins and technology of the advanced extravehicular space suit*. American Astronautical Society, San Diego, CA, 2001.
- [55] J.H Hicks. The mechanics of the foot II. The plantar aponeurosis and the arch. *Journal of Anatomy*, 88(1):25–30, 1954.
- [56] B. Holschuh, J. Waldie, J. Hoffman, and D. Newman. Characterization of structural, volume and pressure components to space suit joint rigidity. In *SAE Technical Papers*. SAE International, 2009.
- [57] Y. P. Ivanenko, R. Grasso, V. Macellari, and F. Lacquaniti. Control of foot trajectory in human locomotion: Role of ground contact forces in simulated reduced gravity. *Journal of Neurophysiology*, 87(6):3070–3089, 2002.
- [58] Ning Ji, Hui Zhou, Kaifeng Guo, Oluwarotimi Williams Samuel, Zhen Huang, Lisheng Xu, and Guanglin Li. Appropriate mother wavelets for continuous gait event detection based on time-frequency analysis for hemiplegic and healthy individuals. *Sensors (Switzerland)*, 19(16):1–18, 2019.
- [59] Ales Jurca and Saso Dzeroski. Length dispersion of shoes labelled with the same size in the UK shoe-size system. *Footwear Science*, 5(SUPPL. 1):2–5, 2013.
- [60] Ales Jurca, Jure Žabkar, and Sašo Džeroski. Analysis of 1.2 million foot scans from North America, Europe and Asia. *Scientific Reports*, 9(1):1–10, 2019.
- [61] W. Kabsch. A solution for the best rotation to relate two sets of vectors. *Acta Crystallographica Section A*, 32(5):922–923, Sep 1976.
- [62] Glen P Kenny, Sean R Notley, and Daniel Gagnon. Direct calorimetry: a brief historical review of its use in the study of human metabolism and thermoregulation. *European Journal of Applied Physiology*, 117:1765–1785, 2017.
- [63] Sarah E. Kessler, Glen A. Lichtwark, Lauren K.M. Welte, Michael J. Rainbow, and Luke A. Kelly. Regulation of foot and ankle quasi-stiffness during human hopping across a range of frequencies. *Journal of Biomechanics*, page 109853, 2020.
- [64] K. Han Kim, Karen Young, Elizabeth Benson, Sarah Jarvis, Linh Vu, Yaritza Hernandez, and Sudhakar Rajulu. Human modeling tools for spacesuit and hardware design and assessment. In Sofia Scataglini and Paul Gunther, editors, *DHM and Posturography*, chapter 46, pages 613–625. Academic Press, jan 2019.
- [65] K. Han Kim, Karen S. Young, Yaritza Bernal, Abhishekha Boppana, Linh Q. Vu, Elizabeth A. Benson, Sarah Jarvis, and Sudhakar L. Rajulu. A Parametric Model of Shoulder Articulation for Virtual Assessment of Space Suit Fit. In *Proceedings of the 7th International Conference on 3D Body Scanning Technologies*, pages 201–207, Lugano, Switzerland, nov 2016.

- [66] Kenneth R King. The SHUTTLE EXTRAVEHICULAR MOBILITY UNIT (EMU): PROVEN HARDWARE FOR SATELLITE SERVICING. In Satellite Service Workshop, number June, Houston, TX, jun 1982. NASA Johnson Space Center.
- [67] Joseph J. Kosmo and Amy Ross. Space suit mobility evaluations in lunar/mars gravity environments. JOURNAL OF AEROSPACE, 107:535–542, jul 1998.
- [68] Joseph J. Kosmo, William E. Spenny, Rob Gray, and Phil Spampinato. Development of the NASA ZPS Mark III 57.2-kN/m² (8.3 psi) space suit. JOURNAL OF AEROSPACE, 1988.
- [69] Makiko Kouchi, Makoto Kimura, and Masaaki Mochimaru. Deformation of foot cross-section shapes during walking. Gait and Posture, 30(4):482–486, nov 2009.
- [70] Rodger Kram, Antoinette Domingo, and Daniel P. Ferris. Effect of reduced gravity on the preferred walk-run transition speed. Journal of Experimental Biology, 200(4):821–826, 1997.
- [71] I. Krauss, S. Grau, M. Mauch, C. Maiwald, and T. Horstmann. Sex-related differences in foot shape. Ergonomics, 51(11):1693–1709, nov 2008.
- [72] Inga Krauss, Gordon Valiant, Thomas Horstmann, and Stefan Grau. Comparison of female foot morphology and last design in athletic footwear—are men's lasts appropriate for women? Research in Sports Medicine, 18(2):140–156, 2010.
- [73] A. Leardini, M. G. Benedetti, L. Berti, D. Bettinelli, R. Nativo, and S. Giannini. Rear-foot, mid-foot and fore-foot motion during the stance phase of gait. Gait and Posture, 25(3):453–462, mar 2007.
- [74] P. Lundgren, C. Nester, A. Liu, A. Arndt, R. Jones, A. Stacoff, P. Wolf, and A. Lundberg. Invasive in vivo measurement of rear-, mid- and forefoot motion during walking. Gait and Posture, 28(1):93–100, 2008.
- [75] Geng Luo, Pro Stergiou, Jay Worobets, Benno Nigg, and Darren Stefanyshyn. Improved footwear comfort reduces oxygen consumption during running. Footwear Science, 1(1):25–29, 2009.
- [76] Ameersing Luximon and Yan Luximon. Shoe-last design innovation for better shoe fitting. Computers in Industry, 60(8):621–628, 2009.
- [77] Y. Luximon and A. Luximon. Sizing and grading of shoe lasts. Handbook of Footwear Design and Manufacture, pages 197–215, 2013.
- [78] E. A. Mailer and B. B. Adams. The wear and tear of 26.2: Dermatological injuries reported on marathon day. British Journal of Sports Medicine, 38(4):498–501, aug 2004.
- [79] Roger A Mann and John L Hagy. The function of the toes in walking and running. Clinical Orthopaedics & Related Research, (142):24–29, 1979.
- [80] Sarah Margerum, Mike Ferrer, Karen Young, and Sudhakar Rajulu. Relating Linear and Volumetric Variables through Body Scanning to Improve Human Interfaces in Space. In International Conference on 3D Body Scanning Technologies, pages 10–22, Lugano, Switzerland, oct 2010.

- [81] Benoit Mariani, Hossein Rouhani, Xavier Crevoisier, and Kamiar Aminian. Quantitative estimation of foot-flat and stance phase of gait using foot-worn inertial sensors. *Gait and Posture*, 37(2):229–234, 2013.
- [82] José M. Martínez-Martínez, José D. Martín-Guerrero, Emilio Soria-Olivas, José A. Bernabeu, Pablo Escandell-Montero, Rafael Hernández Stark, Antonio J. Serrano-López, and Enrique Montiel. Use of SOMs for footwear comfort evaluation. *Neural Computing and Applications*, 28(7):1763–1773, jul 2017.
- [83] Ian M Meginnis, Richard A Rhodes, and Kristine N Davis. Performance of the Z-2 Space Suit in a Simulated Microgravity Environment. In *48th International Conference on Environmental Systems*, number July, Albuquerque, NM, jul 2018.
- [84] Valentin Menendez, Xavier Labourdette, and Jose Manuel Baez. Performance of EVA suit mobility joints influence of driving parameters. In *SAE Technical Papers*. SAE International, jul 1993.
- [85] Alberto E. Minetti, Gaspare Pavei, and Carlo M. Biancardi. The energetics and mechanics of level and gradient skipping: Preliminary results for a potential gait of choice in low gravity environments. *Planetary and Space Science*, 74(1):142–145, dec 2012.
- [86] A. Mündermann, D. J. Stefanyshyn, and B. M. Nigg. Relationship between footwear comfort of shoe inserts and anthropometric and sensory factors. *Medicine and Science in Sports and Exercise*, 33(11):1939–1945, 2001.
- [87] NASA. Anthropometry and Biomechanics. In *NASA-STD-3000 Man-Systems Integration Standards Volume I*, volume 1, chapter 3. Houston, TX, 1995.
- [88] NASA. Small Business Innovation Research (SBIR) & Small Business Technology Transfer (STTR) Fiscal Year 2019 General Solicitation. 2019.
- [89] Dava Newman and Michael Barratt. Life support and performance issues for extravehicular activity (EVA). In Susanne Churchill, editor, *Fundamentals of Space Life Sciences*, volume 11, chapter 22, pages 1–61. Krieger Publishing Co., Malabar, FL, 1997.
- [90] Dava J. Newman and Harold L. Alexander. Human locomotion and workload for simulated lunar and Martian environments. *Acta Astronautica*, 29(8):613–620, 1993.
- [91] JR Norcross, KG Clowers, Tim Clark, Lauren Harvill, Richard M. Morency, Leah C. Stroud, Jessica R. Vos, and Michael L. Gernhardt. Metabolic Costs and Biomechanics of Level Ambulation in a Planetary Suit. Technical Report February, Houston, TX, 2010.
- [92] J.R. Norcross, L.R. Lee, K.G. Clowers, R.M. Morency, L. Desantis, J.K. DeWitt, J.A. Jones, J.R. Voss, and M.L. Gernhardt. Feasibility of Performing a Suited 10-km Ambulation on the Moon - Final Report of the EVA Walkback Test (EWT). Technical report, Houston, TX, 2009.
- [93] G Oladipo, I Bob-Manuel, and G Ezenatein. Different Weight Bearing Conditions Amongst Nigerians. *The Internet Journal of Biological Anthropology*, 3(1):1–7, 2008.
- [94] Padhraig F. O'Loughlin, Christopher D. Murawski, Christopher Egan, and John G. Kennedy. Ankle instability in sports. *The Physician and Sportsmedicine*, 37(2):93–103, jun 2009.

- [95] Roedolph A. Opperman, James M.A. Waldie, Alan Natapoff, Dava J. Newman, and Jeffrey A. Jones. Probability of spacesuit-induced fingernail trauma is associated with hand circumference. *Aviation Space and Environmental Medicine*, 81(10):907–913, oct 2010.
- [96] Byoung Keon Park and Matthew P. Reed. Parametric body shape model of standing children aged 3–11 years. *Ergonomics*, 58(10):1714–1725, oct 2015.
- [97] Byoung Keon D. Park, Sheila Ebert, and Matthew P. Reed. A parametric model of child body shape in seated postures. *Traffic Injury Prevention*, 18(5):533–536, 2017.
- [98] D. G. Parry, L. R. Curry, D. B. Hanson, and G. B. Towle. A study of techniques and equipment for the evaluation of extravehicular protective garments. Technical report, Wright-Patterson Air Force Base, Dayton, OH, 1966.
- [99] Fabian Pedregosa, Ron Weiss, Matthieu Brucher, Gaël Varoquaux, Alexandre Gramfort, Vincent Michel, Bertrand Thirion, Olivier Grisel, Mathieu Blondel, Peter Prettenhofer, Ron Weiss, Vincent Dubourg, Jake Vanderplas, Alexandre Passos, David Cournapeau, Matthieu Brucher, Matthieu Perrot, Édouard Duchesnay, L. Buitinck, G. Louppe, Olivier Grisel, Fabian Pedregosa, and A. Mueller. Scikit-learn: Machine Learning in Python. *Journal of Machine Learning Research*, 12(85):2825–2830, 2011.
- [100] David S Portree and Robert C Trevino. *Walking to Olympus: An EVA Chronology*, volume 1. NASA History Office, Washington, DC, 1997.
- [101] Carina Price and Christopher Nester. Foot dimensions and morphology in healthy weight, overweight and obese males. *Clinical Biomechanics*, 37:125–130, 2016.
- [102] John R. Rebula, Lauro V. Ojeda, Peter G. Adamczyk, and Arthur D. Kuo. Measurement of foot placement and its variability with inertial sensors. *Gait and Posture*, 38(4):974–980, 2013.
- [103] Matthew P. Reed and Matthew B. Parkinson. Modeling variability in torso shape for chair and seat design. *Proceedings of the ASME Design Engineering Technical Conference*, 1(PARTS A AND B):561–569, 2008.
- [104] M.P. Reed, Ulrich Raschke, Rishi Tirumali, and M.B. Parkinson. Developing and Implementing Parametric Human Body Shape Models in Ergonomics Software. *3rd Digital Human Modeling Symposium*, (1):1–8, 2014.
- [105] J.~G.~T. Ribeiro and J.~L.~F. Freire. Some Comments on Digital Integration to Measure Displacements Using Accelerometers, #130. In *Proceedings of the 17th International Modal Analysis Conference*, volume 3727 of *Society of Photo-Optical Instrumentation Engineers (SPIE) Conference Series*, page 554, mar 1999.
- [106] Deborah Riebe, Barry A. Franklin, Paul D. Thompson, Carol Ewing Garber, Geoffrey P. Whitfield, Meir Magal, and Linda S. Pescatello. Updating ACSM’s recommendations for exercise preparticipation health screening. *Medicine and Science in Sports and Exercise*, 47(11):2473–2479, nov 2015.
- [107] Amy J. Ross, Joseph J. Kosmo, Nikolay Moiseyev, Anatoly Stoklitsky, Daniel Barry, and Edward Hodgson. Comparative space suit boot test. In *SAE Technical Papers*, number 724, 2002.

- [108] Radu Bogdan Rusu and Steve Cousins. 3D is here: Point Cloud Library (PCL). In Proceedings - IEEE International Conference on Robotics and Automation, Shanghai, China, 2011.
- [109] Richard A. Scheuring, Jeffrey A. Jones, Joseph D. Novak, James D. Polk, David B. Gillis, Josef Schmid, James M. Duncan, and Jeffrey R. Davis. The Apollo Medical Operations Project: Recommendations to improve crew health and performance for future exploration missions and lunar surface operations. Acta Astronautica, 63(7-10):980–987, oct 2008.
- [110] Richard A. Scheuring, Charles H. Mathers, Jeffrey A. Jones, and Mary L. Wear. Musculoskeletal injuries and minor trauma in space: Incidence and injury mechanisms in U.S. astronauts. Aviation Space and Environmental Medicine, 80(2):117–124, feb 2009.
- [111] Richard a. Scheuring, P. McCulloch, Mary Van Baalen, C Minard, R Watson, S Bowen, and Terri Blatt. Shoulder injuries in US astronauts related to EVA suit design. In Aerospace Medical Association 83rd Annual Scientific Meeting, Atlanta, GA, may 2012.
- [112] Patricia Schmidt. An Investigation of Space Suit Mobility With Applications to EVA Operations. PhD thesis, Massachusetts Institute of Technology, Cambridge, MA, sep 2001.
- [113] Stephen H. Scott and David A. Winter. Biomechanical model of the human foot: Kinematics and kinetics during the stance phase of walking. Journal of Biomechanics, 26(9):1091–1104, 1993.
- [114] Lakshmi Prabha Nattamai Sekar, Alexander Santos, and Olga Beltramello. IMU drift reduction for augmented reality applications. In Lecture Notes in Computer Science, volume 9254, pages 188–196. Springer Verlag, 2015.
- [115] Young Young Shen and Allison P. Anderson. Extended Kalman Filter for Magnetometer-Free Estimation of Spacesuit Wearer Joint Kinematics Using Inertial Measurements. In FUSION 2019 - 22nd International Conference on Information Fusion, Ottawa, Canada, 2019.
- [116] Young-Young Shen, Shaylah Wood, and Allison P. Anderson. Evaluation of Wearable Inertial Sensors for Spacesuit Design Applications Using Hardware-in-the-Loop Simulation. In AIAA Scitech 2020 Forum, Reston, Virginia, jan 2020. American Institute of Aeronautics and Astronautics.
- [117] Kristina Stanković, Toon Huysmans, Femke Danckaers, Jan Sijbers, and Brian G. Booth. Subject-specific identification of three dimensional foot shape deviations using statistical shape analysis. Expert Systems with Applications, 151:113372, aug 2020.
- [118] Darren J. Stefanyshyn and Benno M. Nigg. Mechanical energy contribution of the metatarsophalangeal joint to running and sprinting. Journal of Biomechanics, 30(11-12):1081–1085, nov 1997.
- [119] Leia Stirling, Damian Kelty-Stephen, Richard Fineman, Monica L.H. Jones, Byoung Keon Daniel Park, Matthew P. Reed, Joseph Parham, and Hyeg Joo Choi. Static, Dynamic, and Cognitive Fit of Exosystems for the Human Operator. Human Factors, 62(3):424–440, 2020.
- [120] Samuel Strauss. Extravehicular Mobility Unit Training Suit Symptom Study Report. Technical Report March, NASA Johnson Space Center, Houston, TX, 2004.

- [121] Samuel Strauss, Ralph L. Krog, and Alan H. Feiveson. Extravehicular mobility unit training and astronaut injuries. *Aviation Space and Environmental Medicine*, 76(5):469–474, may 2005.
- [122] W E Thornton, G Wyckliffe Hoffler, and J A Rummel. Anthropometric changes and fluid shifts. *Biomedical results from Skylab*, NASA SP-37:330–338, 1987.
- [123] Daniele Tomassoni, Enea Traini, and Francesco Amenta. Gender and age related differences in foot morphology. *Maturitas*, 79(4):421–427, 2014.
- [124] Steven F. Viegas, David Williams, Jeffrey Jones, Samuel Strauss, and Jonathan Clark. Physical demands and injuries to the upper extremity associated with the space program. *Journal of Hand Surgery*, 29(3):359–366, 2004.
- [125] Alexandra S. Voloshina, Arthur D. Kuo, Monica A. Daley, and Daniel P. Ferris. Biomechanics and energetics of walking on uneven terrain. *Journal of Experimental Biology*, 216(21):3963–3970, nov 2013.
- [126] John W. Wannop, Darren J. Stefanyshyn, Robert B. Anderson, Michael J. Coughlin, and Richard Kent. Development of a Footwear Sizing System in the National Football League. *Sports Health*, 11(1):40–46, 2019.
- [127] John W. Wannop, Jay T. Worobets, Rodrigo Ruiz, and Darren J. Stefanyshyn. Footwear traction and three-dimensional kinematics of level, downhill, uphill and cross-slope walking. *Gait and Posture*, 40(1):118–122, 2014.
- [128] David R Williams and Brian J Johnson. EMU Shoulder Injury Tiger Team Report. Technical Report September, Houston, TX, 2003.
- [129] P. Wolf, A. Stacoff, A. Liu, C. Nester, A. Arndt, A. Lundberg, and E. Stuessi. Functional units of the human foot. *Gait and Posture*, 28(3):434–441, 2008.
- [130] R. E. Wunderlich and P. R. Cavanagh. Gender differences in adult foot shape: Implications for shoe design. *Medicine and Science in Sports and Exercise*, 33(4):605–611, apr 2001.
- [131] Shuping Xiong, Ravindra S. Goonetilleke, Jianhui Zhao, Wenyan Li, and Channa P. Witana. Foot deformations under different load-bearing conditions and their relationships to stature and body weight. *Anthropological Science*, 117(2):77–88, 2009.
- [132] In-Kwon Yeo and Richard A Johnson. A new family of power transformations to improve normality or symmetry. *Biometrika*, 87(4):954–959, dec 2000.
- [133] Karl E. Zelik and Eric C. Honert. Ankle and foot power in gait analysis: Implications for science, technology and clinical assessment. *Journal of Biomechanics*, 75:1–12, 2018.
- [134] Ju Zhang, Jacqui Hislop-Jambrich, and Thor F. Besier. Predictive statistical models of baseline variations in 3-D femoral cortex morphology. *Medical Engineering and Physics*, 38(5):450–457, 2016.
- [135] Qian-Yi Zhou, Jaesik Park, and Vladlen Koltun. Open3D: A Modern Library for 3D Data Processing. [arXiv:1801.09847](https://arxiv.org/abs/1801.09847), 2018.
- [136] Hui Zou and Trevor Hastie. Regularization and variable selection via the elastic net. *Journal of the Royal Statistical Society. Series B: Statistical Methodology*, 67(2):301–320, 2005.